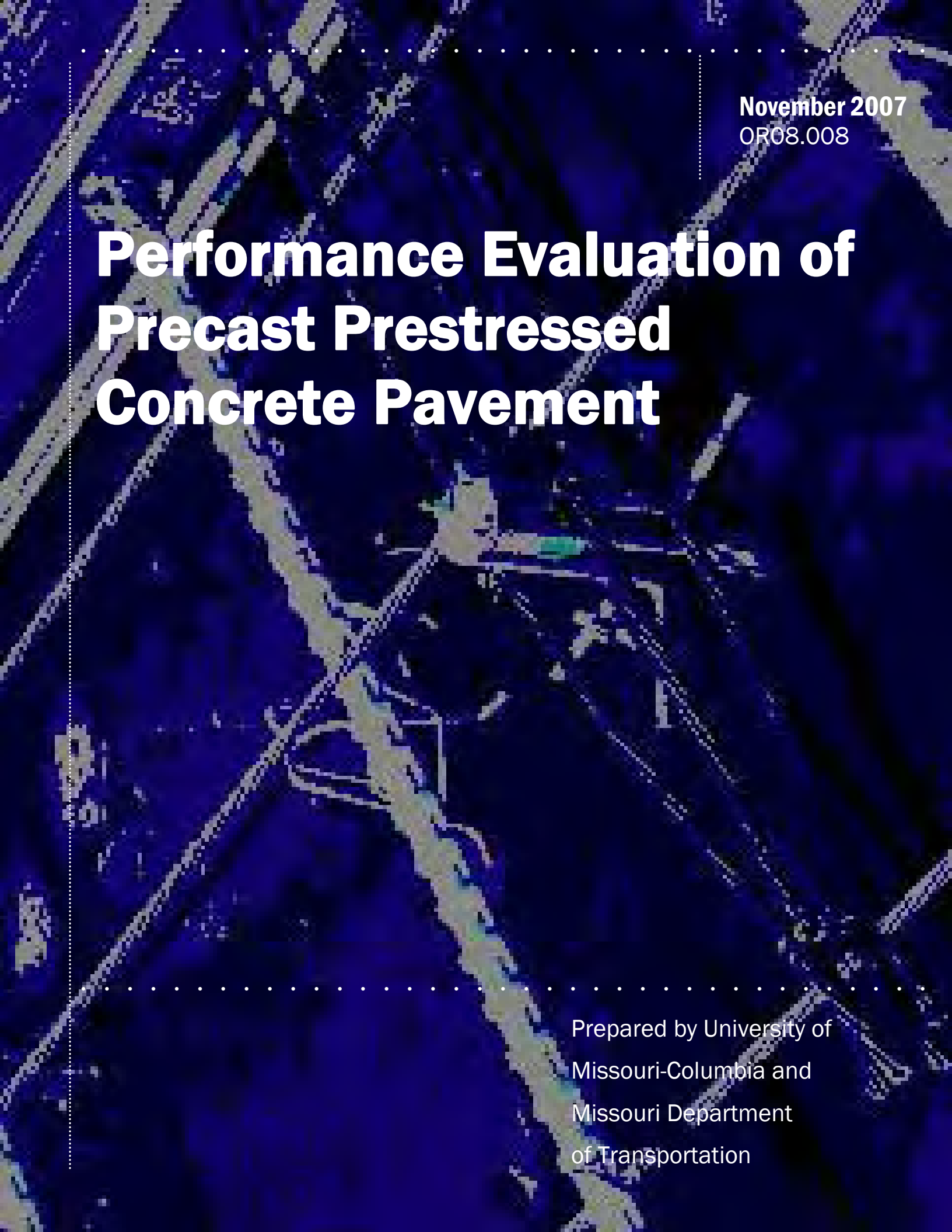

November 2007
OR08.008

Performance Evaluation of Precast Prestressed Concrete Pavement

Prepared by University of Missouri-Columbia and Missouri Department of Transportation

FINAL REPORT
RI03-007

Performance Evaluation of Precast Prestressed Concrete Pavement

Prepared for the
Missouri Department of Transportation
Organizational Results

by

University of Missouri – Columbia
Vellore Gopalaratnam, Professor
Brent M. Davis, M.S.
Cody L. Dailey, M.S.
Grant C. Luckenbill, M.S. Candidate

November 2007

TECHNICAL REPORT DOCUMENTATION PAGE

1. Report No. OR08-008	2. Government Accession No.	3. Recipient's Catalog No.
4. Title and Subtitle Performance Evaluation of Precast Prestressed Concrete Pavement		5. Report Date November 2007
		6. Performing Organization Code
7. Author(s) Vellore Gopalaratnam, Professor, Brent M. Davis, M.S., Cody L. Dailey, M.S. Grant C. Luckenbill, M.S. Candidate		8. Performing Organization Report No. OR08-008/RI03-007
9. Performing Organization Name and Address University of Missouri – Columbia		10. Work Unit No.
		11. Contract or Grant No. RI03-007
12. Sponsoring Agency Name and Address Missouri Department of Transportation Organizational Results P. O. Box 270-Jefferson City, MO 65102		13. Type of Report and Period Covered Final Report
		14. Sponsoring Agency Code MoDOT

15. Supplementary Notes
The investigation was conducted in cooperation with the U. S. Department of Transportation, Federal Highway Administration.

16. Abstract
This report describes in detail an experimental investigation of an innovative precast prestressed concrete pavement (PPCP) system used to rehabilitate a 1,000 ft. section of interstate highway located on the northbound lanes of I-57 near Charleston, MO. The primary objective of this research was to evaluate the performance of the PPCP subjected to severe weather and traffic conditions and develop performance data useful for future projects. The primary difference in this FHWA-MoDOT project compared to other recently completed FHWA projects in Texas and California using the same technology was the incorporation of instrumented pavement panels to quantify pavement performance.

17. Key Words Precast, prestressed, concrete, PPCP, concrete panels	18. Distribution Statement No restrictions. This document is available to the public through National Technical Information Center, Springfield, Virginia 22161

19. Security Classification (of this report) Unclassified	20. Security Classification (of this page) Unclassified	21. No. of Pages 266	22. Price

Form DOT F 1700.7 (06/98)

ACKNOWLEDGEMENTS

The authors would like to gratefully acknowledge support for the instrumentation and monitoring project from the Missouri Department of Transportation (MoDOT). Funding for the project was routed through the Missouri Transportation Institute (Research Project RI003-007). The construction of the experimental pavement section was made possible as a result of funding from the Federal Highway Administration (FHWA) and the MoDOT. Special thanks go to Suneel Vanikar, Mark Swunland and Sam Tyson of FHWA and John Donahue of MoDOT who saw the opportunity for this large scale implementation in Missouri of a relatively new technology. The engineering design support for the project was provided by the Transtec Group. Dave Merrit of the Transtec Group was very helpful in discussions on the instrumentation and monitoring plans of the research team. The research team appreciates the very active and timely assistance on the project from the MoDOT engineers from District 10 office in Sikeston, MO including Eric Krapf, Michael Chasteen, Terry Fields, Marc Scheffel, Barry Horst, Jim Copeland, Craig Compas, and Nathan Conner. Finally, our early-age and construction monitoring would not have been possible without enthusiastic support from Andrew Maybee of Concrete Products Incorporated, Memphis, TN and Harry Neumann of Gaines Construction

EXECUTIVE SUMMARY

This report describes in detail an experimental investigation of an innovative precast prestressed concrete pavement (PPCP) system used to rehabilitate a 1,000 ft. section of interstate highway located on the northbound lanes of I-57 near Charleston, MO. The primary objective of this research was to evaluate the performance of the PPCP subjected to severe weather and traffic conditions and develop performance data useful for future projects. The primary difference in this FHWA-MoDOT project compared to other recently completed FHWA projects in Texas and California using the same technology was the incorporation of instrumented pavement panels to quantify pavement performance. Specific goals within the above broad objective included:

- Study of early age behavior of prestressed panels including; hydration and shrinkage effects, potential residual stresses, and transfer of pre-tensioning.
- Understanding the behavior of joint, anchor, and base panels at various stages of fabrication, construction and service performance.
- Study of prestress losses during post-tensioning and under service conditions.
- Evaluation of the overall performance of individual panels and the interaction of the panels within the system. Specifically performance under traffic loads, and daily and seasonal thermal effects.

Precast panels were fabricated beginning July 2005, construction of the pavement was completed in December 2005 and the highway was opened to traffic in mid January 2006. Seven of the 101 pavement panels were instrumented and monitored during the various stages from panel fabrication in July 2005 to performance under service loads until May 2007. Thirty-nine strain gage instrumented rebars, fourteen vibrating wire gages, four strandmeters, and thirty-eight thermocouples were installed in the seven instrumented panels. The instrumentation and data acquisition system developed facilitated remote monitoring of the pavement once in service. Companion laboratory studies were performed to characterize concrete properties for analysis of results for the

field measurements. Laboratory studies included compressive strength, modulus of rupture, fracture energy, chloride permeability, freeze-thaw resistance, unrestrained creep and unrestrained shrinkage tests.

The project successfully demonstrated the remote service monitoring capability of the data acquisition system. It has been shown that with appropriate data acquisition rates, monitoring of related embedded instrumentation, and methods of analysis, it was possible to isolate and measure strains from traffic loads, prestress losses due to viscous effects such as creep, shrinkage and relaxation, daily strain excursions due to day-night thermal loads, pavement strains due to local weather fronts lasting a few days or weeks and seasonal variations lasting several months of cooling or heating trends. Pavement strains due to temperature changes significantly overshadow strains due to all other types of loading (viscous effects such as creep, shrinkage and relaxation, or vehicular loads).

Several suggestions are made based on observations from the study to improve the fabrication and construction processes used. Early age behavior during hydration/curing has been discussed. Concrete strains due to progressive prestress transfer during panel fabrication as well as post-tensioning operations during construction have been studied and analyzed. Significant pavement characteristics are identified based on experimental data from service performance on the influence of daily, short-term and seasonal thermal loading. Long-term prestress losses due to viscous effects such as creep, shrinkage and relaxation have been estimated and compared with theoretical predictions using an incremental time-step model.

TABLE OF CONTENTS

LIST OF TABLES

LIST OF FIGURES

NOMENCLATURE /LIST OF NOTATION

A_c – AREA OF CONCRETE CROSS-SECTION

A_{ps} – AREA OF PRESTRESSING STEEL

E_{ps} – MODULUS OF ELASTICITY OF PRESTRESSING STRANDS

$(f_{cgp})_{FJ}$ – STRESS IN CONCRETE AT THE CENTROID OF PRESTRESSING TENDONS DUE TO PRESTRESSING FORCE

$(f_{cgp})_G$ – STRESS IN CONCRETE AT CENTROID DUE TO SELF-WEIGHT

f_{pi} – INITIAL PRESTRESSING FORCE

f_{py} – YIELD STRENGTH OF STEEL

f_{pJ2} – INITIAL STRESS IN PRESTRESSING TENDON AT END OF STRESSING

Δf_{pC} – CHANGE IN PRESTRESSING FORCE DUE TO CREEP

Δf_{pES} – CHANGE IN APPLIED FORCE DUE TO ELASTIC SHORTENING

Δf_{pR1} – STRAND RELAXATION AT ANY TIME AFTER STRESSING

Δf_{pS} – CHANGE IN PRESTRESSING FORCE DUE TO SHRINKAGE

Δf_{pR} – CHANGE IN PRESTRESSING FORCE DUE TO RELAXATION

Δf_{pT} – TOTAL CHANGE IN PRESTRESSING FORCE

n_p – MODULAR RATIO

n_{pi} – INITIAL MODULAR RATIO

E_R – Relative Modulus of Elasticity (Freeze/Thaw)

P – APPLIED LOAD

t – TIME

δ – DEFLECTION

ε_{sh} – SHRINKAGE STRAIN

ε_{sh}^{*} – SHRINKAGE STRAIN AT TIME INFINITY

σ – STRESS

$\gamma_{1-}\gamma_{7}$ – CORRECTION FACTORS FOR RELATIVE HUMIDITY, MEMBER SIZE AND SHAPE, CONCRETE SLUMP, FINE AGGREGATE TO TOTAL AGGREGATE RATIO, AIR CONTENT, CEMENT CONTENT, AND INITIAL CURING PERIOD

JCP – JOINTED CONCRETE PAVEMENT

JRCP – JOINTED REINFORCED CONCRETE PAVEMENT

CRCP – CONTINUOUSLY REINFORCED CONCRETE PAVEMENT

PPCP – PRECAST PRESTRESSED CONCRETE PAVEMENT

AASHTO – AMERICAN ASSOCIATION OF STATE HIGHWAY AND TRANSPORTATION OFFICIALS

ADT – AVERAGE DAILY TRAFFIC

FHWA – FEDERAL HIGHWAY ADMINISTRATION

ETG – EXPERT TASK GROUP

CPI – CONCRETE PRODUCTS INCORPORATED

PVC – POLYVINYL CHLORIDE

ASTM – AMERICAN SOCIETY FOR TESTING AND MATERIALS STANDARD

ACPA – AMERICAN CONCRETE PAVEMENT ASSOCIATION

MODOT – MISSOURI DEPARTMENT OF TRANSPORTATION

BN – INSTRUMENTED BASE PANEL LABEL (NUMBER 'N')

CN – INSTRUMENTED ANCHOR PANEL LABEL (NUMBER 'N')

A3N – INSTRUMENTED JOINT PANEL LABEL (NUMBER 'N')

RN – INSTRUMENTED REBAR LABEL (NUMBER 'N')

VN – VIBRATING WIRE GAGE LABEL (NUMBER 'N')

SN – STRANDMETER LABEL (NUMBER 'N')

TN – THERMOCOUPLE LABEL (NUMBER 'N')

VNt – VIBRATING WIRE GAGE THERMISTOR LABEL (NUMBER 'N')

SNt – STRANDMETER THERMISTOR LABEL (NUMBER 'N')

KIP – 1,000 POUNDS

HZ – HERTZ (UNIT FOR FREQUENCY)

MV – MILLI-VOLTS

μSTR – MICROSTRAIN

°C – DEGREES CENTIGRADE

°F – DEGREES FAHRENHEIT

DC – DIRECT CURRENT

AC – ALTERNATING CURRENT

DAQ – DATA ACQUISITION

DSL – DIGITAL SUBSCRIBER LINE

RTDM – REAL TIME DATA MONITORING

LVDT – LINEAR VARIABLE DISPLACEMENT TRANSDUCERS

RCPT – RAPID CHLORIDE PERMEABILITY TEST

KN – KILONEWTON

MPA – MEGAPASCAL

f_r – MODULUS OF RUPTURE FOR CONCRETE

G_f – FRACTURE ENERGY (CONCRETE)

SSD – SATURATED SURFACE DRY

CTE – COEFFICIENT OF THERMAL EXPANSION

CTC – COEFFICIENT OF THERMAL CONTRACTION

T – TEMPERATURE

t – TIME

ε – STRAIN

R – REBAR STRAIN READING

ΔL_{UC} – UNRESTRAINED CONCRETE EXPANSION (DUE TO ΔT)

ΔL_{US} – UNRESTRAINED STEEL REBAR EXPANSION (DUE TO ΔT)

ΔL_{R} – RESTRAINED STEEL REBAR EXPANSION (DUE TO ΔT)

PSI – POUNDS PER SQUARE INCH

P – FORCE IN PRESTRESSING STRAND

A – AREA OF CONCRETE CROSS SECTION

y – DISTANCE FROM THE NEUTRAL AXIS TO A SPOT IN THE CROSS-SECTION

I – MOMENT OF INERTIA

f_{pi} – INITIAL PRESTRESSING STRESS

f_{pu} – ULTIMATE PRESTRESSING STRESS

F_{plf} – FORCE IN STRAND PER LINEAR FOOT

α – COEFFICIENT OF THERMAL EXPANSION

M – MOMENT

d – DEPTH OF PANEL

w – WIDTH OF PANEL

e – INTERNAL ECCENTRICITY OF STRESSED STRAND

N.A. – NEUTRAL AXIS

E – MODULUS OF ELASTICITY

ν – POISON'S RATIO

n – NUMBER OF STRANDS STRESSED AT A GIVEN TIME

CJC – COLD JUNCTION COMPENSATION

UPS – UNINTERRUPTIBLE POWER SUPPLY

1. Introduction

1.1. Motivation for a Precast, Prestressed Pavement Program

The appetite over recent years for more durable and longer lasting roadway systems has been growing. With increasing traffic volumes, tire pressures, and truck weights becoming the norm, designers have to contend with the need to upgrade current roadways and seek more cost-effective means of pavement rehabilitation.

Precast, prestressed concrete pavement (PPCP) technology although relatively new has only been explored on small scale projects until recently. Design of large-scale PP systems and their practical implementation requires research involving analytical procedures are well as experimental validation. Many of the design methods for PPCP were adapted from the design of other prestressing applications such as bridge girders or post-tensioned slabs. Other PPCP projects were platforms for designers to explore the use of precast pavements for rapid replacement. Research is needed to develop robust design and construction methodology that can be routinely implemented for repairs as well as new construction. Data from embedded instrumentation can be used to verify assumptions made during design, and will facilitate development of design standards. Authentication of design methods through performance measures will give designers the validation for future projects.

Hands-on experience for contractors is vital in developing new technology. During construction, contractors develop the skills and procedures necessary to complete designs and also demonstrate to other contractors the ability to complete the project.

1.1.1. MODOT Precast Project in Sikeston

The state of Missouri demonstrated a commitment to developing PPCP technology by jointly funding a new test section in cooperation with the FHWA. The Missouri PPCP test section is located on the northbound lanes of I-57 near Charleston, MO. The project was completed in December, 2005 and opened to traffic in mid January, 2006.

The charge of the Missouri project was to advance technologies developed in recently completed projects near Georgetown, TX and El Monte, CA. The previous projects displayed that designers and contractors can make PPCP work. By choosing to do a project in southern Missouri, the pavement would have to endure extreme environmental conditions. Missouri is known for sustaining harsh winters, blistering summers, and pavements are subject to de-icing salts. Heavy truck traffic on I-57, (approximately 30% trucks), could significantly affect the durability of PPCP in such severe environmental conditions.

1.2. Research Goals

1.2.1. Research Objectives

The primary objective of the University of Missouri-Columbia was to evaluate the performance of the PPCP subjected to severe weather and traffic conditions and develop performance data useful for future projects. The primary difference in the Missouri pilot project compared with recently completed projects was the incorporation of instrumented pavement panels to quantify pavement performance and validate design approach. Specific goals within the above broad objectives included:

- Study of early age behavior of prestressed panels. Parameters investigated included; hydration and shrinkage effects, residual stresses, and transfer of pre-tensioning.
- Understanding the behavior of joint, anchor, and base panels at various stages of construction and service performance.
- Study of prestress losses during post-tensioning and under service conditions.
- Evaluation of the overall performance of individual panels and the interaction of the panels within the system. Specifically curling at joints, chloride ingress, performance under traffic loads, and daily and seasonal thermal effects.

Laboratory studies were performed to characterize concrete properties for analysis of results for the field measurements. Concrete compressive strength and modulus were determined to ensure the mix design met specified requirements. Unrestrained creep and shrinkage was studied to quantify losses in both prestressing and post-tensioning of the concrete. Deicing salts are readily used on pavements in Missouri; therefore baseline chloride permeability tests were performed on virgin pavement concrete with in-service values to facilitate later comparisons. Large temperature fluctuations are also commonplace in southeastern Missouri; with several freeze-thaw cycles during each winter as a result the concrete was subjected to rapid freezing and thawing to test its long-term durability. Finally, flexure tests were conducted to determine the flexural tensile strength and fracture toughness of the concrete.

1.2.2. Early age Response of Precast Panels

Curing temperatures and corresponding strains were measured to help understand early age curing and hydration response of the panel in unique steel forms. A high

cement content mix design in conjunction with steam curing ensured quick turn around on molds allowing the precaster, CPI in Memphis, TN, to cast new panels every day. Large internal temperatures were observed during hydration due to a combination of heat of hydration and steam curing. These factors significantly influence early age shrinkage strains. Hardened concrete, expands and contracts with increases and decreases in temperature respectively. The geometry of the PPCP panel has a high surface area to volume ratio and is subjected to significant frictional restraint. Frictional restraint, early age shrinkage, and thermal gradients while curing have the potential to cause residual strain in the panels. Early age temperature and strain distributions measured in this investigation facilitate computation of these stresses.

Transfer of pre-tensioning force is a critical loading stage in the life of the one day old panel. The pre-tensioning strands for the Missouri pilot project were designed to accommodate the varying depth cross-section while minimizing eccentricity. Experimentally measured strains are later compared to analytical predictions. It is necessary to monitor the strains produced during transfer to further understand the relationship of prestressing and early-age stresses due to temperature, friction, and shrinkage. Concrete strains measured at prestress transfer validate the design assumptions and also provide for a base line reading for time-dependent prestress loss investigation.

1.2.3. Prediction and Verification of Prestress Losses

The pre-compression influenced creep response of the panels. Drying and hydration influence shrinkage of the panels. Both creep and shrinkage affect the level of prestress during the lifetime of the pavement. Accurate prediction of prestress losses due

to creep and shrinkage is needed to ensure PPCP will perform as desired. Results from multiple laboratory studies are utilized in appropriate models used to predict prestress losses. For example, comparing predicted losses due to creep through experimental methods will validate parameters input into the models used for pre and post-tension loss prediction in the concrete.

As stated earlier, optimizing the use of concrete by applying a pre-compressive force is advantageous with regards to long-term durability and economical use of concrete. However, it is important to understand the decrease or loss of this applied force over time. Multiple models exist to predict loss of stress in prestressing or post-tensioning strands. An incremental time-step model that accounts for the coupled effects due to creep and shrinkage allowed a study of prestress loss with time. This, coupled time-step model took into account not only creep and shrinkage of the concrete but also relaxation, elastic shortening of the strand and friction between the strand and concrete. A comparison between predicted total post-tensioning loss evaluated from creep and shrinkage laboratory experiments and relaxation models with field measurement of total post-tensioning loss has been completed in this study as described later.

1.2.4. Service Performance

The influence of ambient temperature fluctuations controls a large portion of the design (Merritt, McCullough et al. 2000). Once each section of panels is post-tensioned, they act as a 250’ long composite section. Understanding the thermal displacements in the 250’ sections is necessary in characterizing the performance of the pavement. This is more critical during decreases in temperature because the slab contracts. As the slab contracts, friction against the base will cause tensile forces. Service investigations show

temperature and corresponding strain variations. Strain from traffic and daily/seasonal temperature gradients are monitored continuously to understand service performance of the pavement system. Global movement of the sections due to thermal or sub-grade moisture variations and consolidation were evaluated during the early service of the pavement using a GPS total station. These were later discontinued due to poor resolution of their measurements.

1.2.5. Long Term Performance

Long term performance consists of correlating creep and shrinkage prediction models, measured unrestrained creep and shrinkage, and actual losses observed. Prestress losses are extrapolated and validated with corresponding prestressing strand strain measurements. Seasonal thermal variations are observed and compared. Visual inspections of the pavement surface for cracking and joint performance were completed during this study.

2. BACKGROUND INFORMATION

2.1. PAST PPCP PROJECTS IN THE USA

The pilot project using PPCP in Missouri addresses several new aspects compared to the earlier experimental projects. The completed pavement projects in Texas and California are located in milder climates and are not subjected to deicing salts. The Missouri project will be subject to significant seasonal as well as daily temperature variations. Furthermore, deicing salts are commonly used for snow/ice removal.

The research completed to date for precast pavements is purely based on knowledge gained through other applications of prestressed and precast concrete. Although extrapolation of details from similar projects is possible, the same assumptions cannot always be made for the application of PPCP. Detailed descriptions of recent PPCP projects are reported in the following sections.

2.1.1. GEORGETOWN, TEXAS

A prestressed precast roadway project in Texas was the first of many planned joint FHWA and state DOT projects involving this new technology. The location for the Texas project was a frontage road along I-35 just north of Georgetown, TX. The Texas project incorporated both full width and partial width panels. The full width panels were post-tensioned longitudinally, and the partial width panels were post-tensioned both longitudinally and horizontally. A total of 339 panels were fabricated, of which 123 were full width and 216 were partial width. The full width panels were wide enough to accommodate two twelve foot lanes an eight foot outside shoulder and a four foot inside shoulder. The partial width panels were 16 feet and 20 feet in width respectively. When

placed, the centerline of the roadway matched with the joint between the two panels. The length of the panels was ten feet, which was controlled by weight restrictions for transportation to the site (Tyson and Merritt 2005).

The pavement in Texas has been in service since March 2002 and has shown no signs of deterioration. Careful planning and the overall success of the project in Georgetown, Texas opened doors for the projects in California and Missouri.

2.1.2. EL MONTE, CALIFORNIA

In April 2004 the California Department of Transportation (Caltrans) completed a project on Interstate 10 near El Monte, CA. This project involved a little more complexity compared with the Texas project by requiring varying cross-slopes cast into the panels, and nighttime construction operation (Tyson and Merritt 2005). The total length of roadway replaced was 250' and consisted of two driving lanes and a 10' shoulder. A total of 31 panels were fabricated and placed over a two night period. The panels were prestressed transverse to the direction of traffic and post-tensioned in two 124' sections longitudinal to traffic (Tyson and Merritt 2005).

2.1.3. SHELDON, IOWA

A challenging Iowa project incorporated the use of partial width precast prestressed pavement panels for bridge approach slabs on Highway 60 near Sheldon, Iowa. Although the roadway was closed, partial width panels were used to simulate "lane by lane" construction to be used in future rehabilitation projects. Two 77' long sections were post-tensioned longitudinally and transversely from the roadway edges upon installation.

2.2. A LOOK AT PPCP AND ALTERNATIVES

PPCP is a viable substitute for repair and replacement of conventional cast in place concrete by minimizing intrusive construction delays on travelers. Traffic congestion due to the presence of construction activities results in, among many other variables, increased fuel consumption and lost work time, or user costs and safety issues related to construction (Merritt 2001). All of which can be mitigated by using PPCP. PPCP allows constructors to perform full depth replacement of roadway during off peak travel times and allows traffic to resume on the newly replaced pavement almost immediately. By avoiding the peak travel times for construction, safety for workers and travelers are improved due to the decreased traffic volumes.

When rigid pavements have been in service for a few years, voids can develop underneath the pavement due to many factors. These voids affect pavement support possibly reducing the life of the pavement under repetitive wheel loading. A prestressed concrete pavement has the ability to "span" these voids like a flexural member due to the pre-compressive stress in the pavement. Simply increasing the prestressing force will help the panel act like a thicker pavement (Merritt, McCullough et al. 2000).

Precast panels typically have better quality control given the fact that they are produced under a relatively controlled environment at a precasting yard. The panels can be cured to help minimize shrinkage effects, and the development of residual stresses. Further investigation into the effects of shrinkage, prestressing, and environmental factors on residual stresses are discussed in a later section.

Use of PPCP for rapid rehabilitation was attempted in the mid 1980's. Projects utilizing prestressed cast in place concrete, in Texas, South Dakota, Pennsylvania, Arizona, and Mississippi have proven very effective.

Load transfer efficiency is another benefit of using precast prestressed panels. When cracks in concrete become larger than 0.03 – 0.04 inches, the pavement can no longer rely on aggregate interlock to provide load transfer and must utilize dowel bars, or other means. This load transfer ability decreases as the cracks increase in size. The reinforcement placed in pavement is to help limit the opening of these cracks. The use of prestressed reinforcement further helps in keeping the cracks closed. The shear friction alone, provided by the pre-compression in a prestressed pavement, provides optimal load transfer across joints and cracks (Merritt, McCullough et al. 2000).

Concrete poured on a base course will tend to have a rough underside, because it takes the shape of the base course, thus increasing the coefficient of friction of the bottom surface of the pavement. Additionally, concrete poured onto the base will be restrained by a larger mechanical means in which small slivers of concrete are allowed to seep in between the aggregates causing small surface irregularities or "fingers" tying the concrete to the base. When the concrete shrinks, the restraint against the base causes residual stresses in the concrete. Temperature changes during the day can also cause concrete pavement to develop stresses against the base. In Missouri, where 20 degree temperature excursions during the day are not uncommon, the temperature differential between the pavement and base can be quite large. The rates of expansion and contraction of the two dissimilar materials coupled with the temperature differential may cause stresses to be induced in the pavement. The placement of polyethylene sheeting is sometimes used to

help mitigate these stresses by providing a smooth barrier for the pavement and base. However, it appears that significant stresses caused by friction between the pavement and base are unavoidable and may cause the roadway to deteriorate sooner than if there were no frictional restraint. Here too, PPCP has an advantage over cast in place concrete by providing a smooth underside mirroring the shape of the steel bed forms, thus minimizing friction with the base.

Benefits for improved safety and reduced user costs while using precast prestressed panels may not be sufficient for full depth replacement projects. In rural areas where traffic congestion is minimal, the user costs would not outweigh the cost of construction using precast panels. However, the use of precast panels is well suited in urban roadway replacement projects. The following sections describe the essential details of three different types of pavement replacement. Three popular techniques exist for rigid pavement construction; Jointed Plain Concrete Pavement (JPCP), Jointed Reinforced Concrete Pavement (JRCP), and Continuously Reinforced Concrete Pavement (CRCP).

2.2.1. JOINTED PLAIN CONCRETE PAVEMENT

JPCP contains no reinforcing steel and contains enough joints to control the location of natural cracks (ACPA 2004). To help in load transfer dowel bars are often used between joints. Figure 2.1 shows an overhead and side view of typical JPCP construction. Dowel bars embedded in the surface course are important to transfer load between joints. JPCP is the most common concrete pavement design in the U.S.

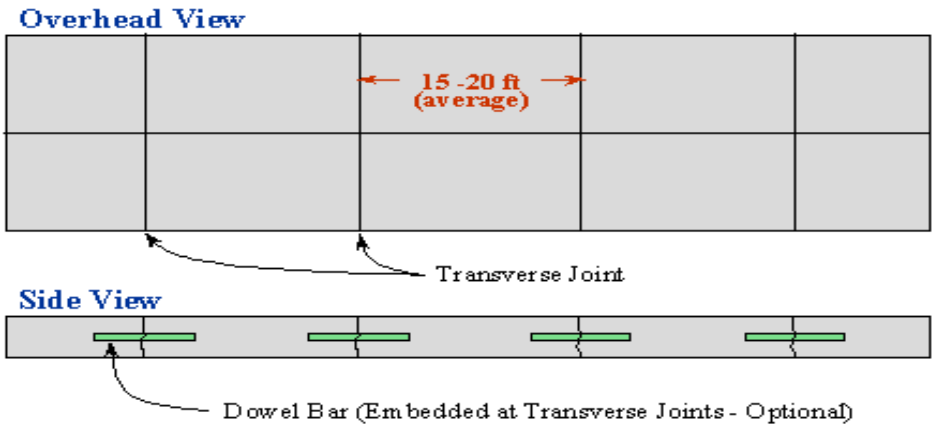

Figure 2.1 – Overhead and side view of Jointed Plain Concrete Pavement (ACPA 2004)

2.2.2. JOINTED REINFORCED CONCRETE PAVEMENT

JRCP is somewhat similar to JPCP; however a reinforcing wire mesh is used to hold cracks together between joints. Normally the joints are spaced at 30 feet or more (ACPA 2004). Figure 2.2 shows cracks that have formed between joints, but because of the wire mesh reinforcement the cracks are held together. JRCP also uses dowel bars between joints for load transfer efficiency (ACPA 2004). Largely attributed to maintenance issues, JRCP is rarely constructed by State DOT's.

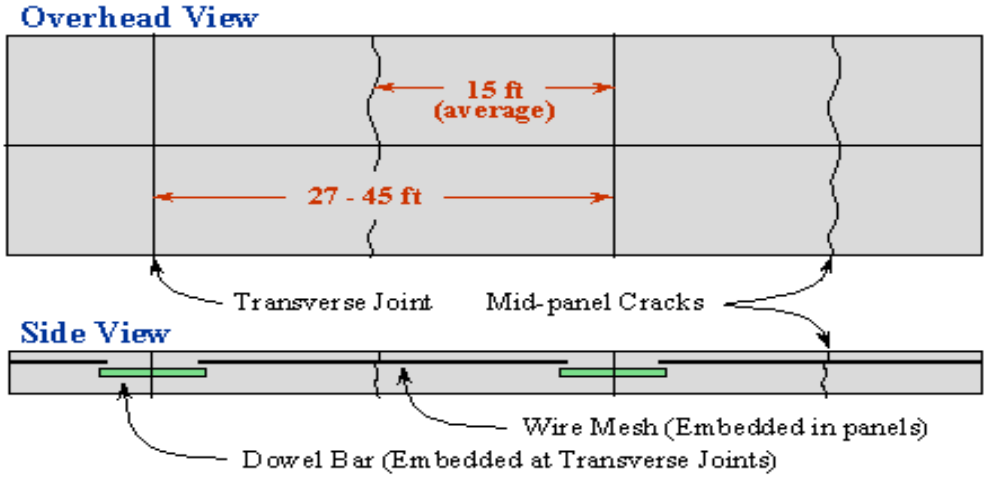

Figure 2.2 – Overhead and side view of Jointed Reinforced Concrete Pavement (ACPA 2004)

2.2.3. CONTINUOUSLY REINFORCED CONCRETE PAVEMENT

CRCP, unlike JPCP and JRCP, requires no transverse joints. Cracks are expected in the slab, but are held together tightly through the use of reinforcing steel (ACPA 2004). When designing, the crack spacing is normally predicted. The cost of CRCP is more than that of JPCP and JRCP, but is justified by its long-term effectiveness (ACPA 2004). Figure 2.3 shows typical CRCP construction and typical cracking patterns. Illinois and Texas often utilize CRCP as their primary concrete pavement design.

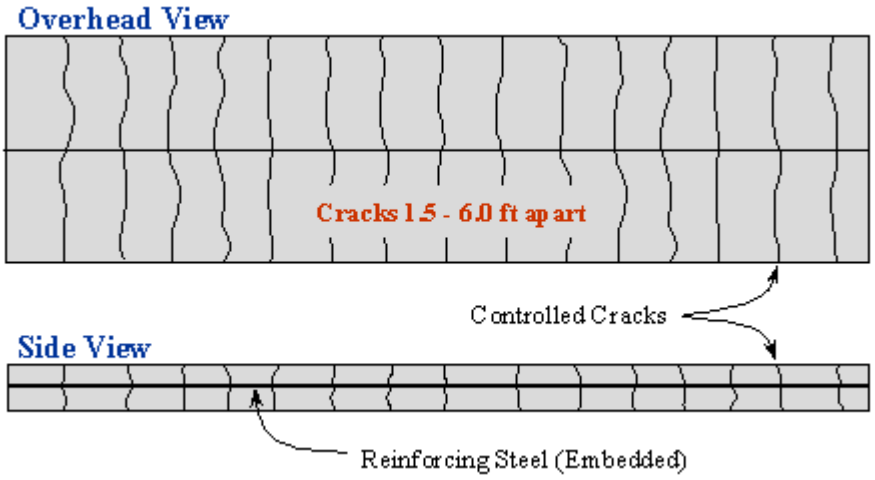

Figure 2.3 – Overhead and side-view of Continuously Reinforced Concrete Pavement (ACPA 2004)

Current rigid pavement replacement practices, although reliable, are directly responsible for lengthy delays and high end user costs. In the past few years, research has been conducted to identify more efficient methods of rigid pavement construction practices. This research has brought to light key issues related to rigid pavement construction. Optimizing material use is a large component in curbing costs associated with any construction venture, especially in large material volume projects such as roadways. If it were possible to make an 8" thick pavement perform like a 14" thick pavement then material costs would be nearly cut in half. Use of prestressing strands can make this possible. Concrete is inherently weak in tension, but very strong in compression. One reason why current pavements are so thick is due to this weakness in tension. Figure 2.4 illustrates how a pavement acts under tire loadings. A possible way to overcome concrete's weakness in tension is to place pre-compression forces where tensile stresses occur. Incorporating compression or prestressing forces in concrete has been successfully used in bridge girder construction, foundation mats, parking structures, and floor systems. Taking lessons learned in these varying applications and applying them to roadway construction may be one viable option for future rigid pavement rehabilitation.

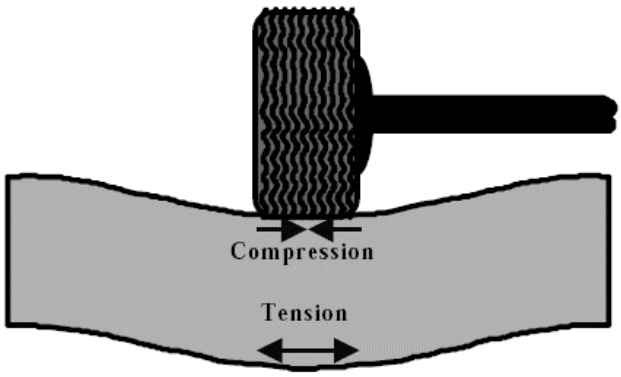

Figure 2.4 – Slab stresses generated from wheel loads (Merritt, McCullough et al. 2000)

3. PROJECT INFORMATION AND CONSTRUCTION

3.1. GENERAL INFORMATION

The Precast Prestressed Concrete Pavement (PPCP) test section in Missouri replaced a dilapidated 45 year old section of cast in place concrete just west of Charleston, MO on north bound I-57 (I-57 actually runs east to west at the PPCP section). Three specific types of panels make up the PPCP system: base panels, joint panels, and anchor panels.

Each panel is 10'-0" x 38'-0" (3 m x 11.6 m). The 38' dimension is perpendicular to traffic. There is a 4'-0" (1.22 m) inside shoulder, two 12'-0" (3.7 m) driving lanes and a 10'-0" (3 m) outside shoulder. The crown starts between the driving lanes and slopes toward the shoulders at 2% to ensure drainage.

A total of 101 ten foot panels replaced 1,010 ft (304.8 m) of conventional cast-in-place pavement. A typical pavement section consists of an anchor panel in the center with 11 or 12 base panels on each side. Base panels act as filler panels, with the number depending upon the design length of each section, while anchor panels contain full depth holes to accommodate dowel bars which are driven into the sub-grade to provide anchorage. Joint panels are located at either end of the section and have expansion joints to allow for thermal movement. Each of the four sections is roughly 250 ft (76.2 m) long. Figure 3.1 shows the layout of the four sections of pavement (the highlighted section is heavily instrumented and will be discussed later in detail. Figure 3.2 shows the layout of panels within each individual section.

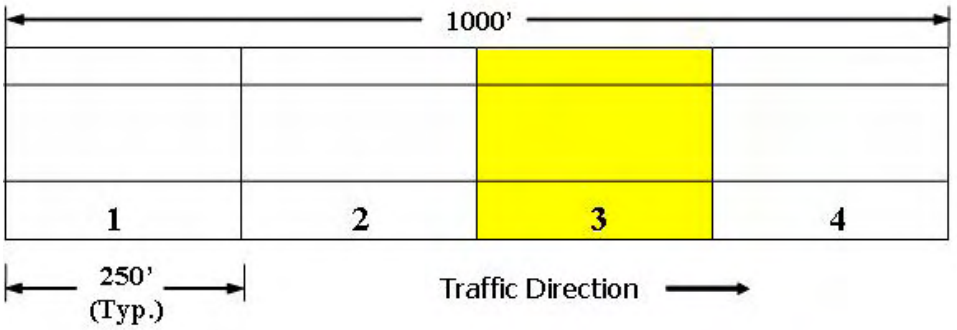

Figure 3.1 – Overall PPCP section layout with driving lanes shown (25 panels per section; Section 3 is heavily instrumented)

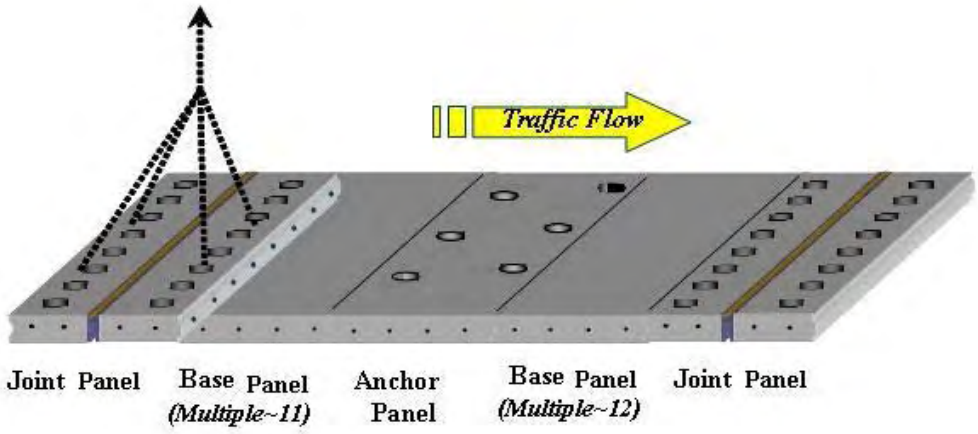

Figure 3.2 – Typical section of PPCP panel assembly and layout modified to reflect Missouri Project (Merritt, McCullough et al. 2000)

3.2. PANEL FABRICATION

All 101 panels were cast by Concrete Products Incorporated (CPI) in Memphis, TN between mid-October and late December 2005. Each panel is pre-tensioned in the transverse direction (perpendicular to traffic). Post-tensioning ducts were installed at 2' on center in the longitudinal direction (parallel to traffic) for desired prestressing and to tie the 250' section together once assembled. The pre-tensioning and post-tensioning forces will create a compressive 'confining effect' on the matrix of the slab that will reduce tensile stresses, prohibit crack growth, and allow for a thinner section compared to

conventional pavement (Tyson and Merritt 2005). Further discussion on this matter was performed by Cody Dailey "Instrumentation and Early Performance of an Innovative Prestressed Precast Pavement System" and Brent Davis "Evaluation of Prestress Losses in an Innovative Prestressed Precast Pavement System."

The panels are post-tensioned through pockets straddling the expansion joint in the joint panel. Male and female shear keys cast into the side of the panels help with load transfer and align the panels during placement and post-tensioning (shear keys extend only to limits of the driving lanes because of insufficient panel thickness in the shoulders). Once in place, post-tensioning strands were fed through the ducts (cast into the panels) and stressed at the joint panels. The ducts were grouted to seal and protect the strands and block-outs were filled. Diamond grinding was performed on the driving lanes for smoothness in ride quality and mitigation of impact/fatigue effects.

3.2.1. PRECAST PANEL DESIGN

The Transtec Group from Austin, TX designed the PPCP system consisting of base, anchor, and joint panels. Transtec design drawings are provided in Appendix A. Panel design was funded by FHWA. The following sections discuss specifications and design details relevant to the fabrication of the precast prestressed panels.

3.2.1.1. BASE PANELS

The base panels make up the majority of the pavement and are placed between the joint panels and central anchor panel. Ninety two base panels were cast. CPI cast most of the base panels first in order to become familiar with the new fabrication process before attempting joint panels which involve more complexities in fabrication. Figure 3.3 shows a plan view of a typical base panel. Regular 60 ksi (414 MPa) epoxy coated

rebar bordered the edges of each panel and is not shown on the schematics. It reinforced the edges and corners where stress concentrations may develop and cause cracking. Each base panel contains eight pre-tensioning strands as shown in Figure 3.3 and Figure 3.4. The strands in the top half of the panel are draped to follow the slope of the crown and meet cover requirements at the shoulders. Draping was done by placing chairs under the top strands at certain places. This raised the strand within the cross section creating uniform and gradient free stress distribution from top to bottom (see Figure 3.5).

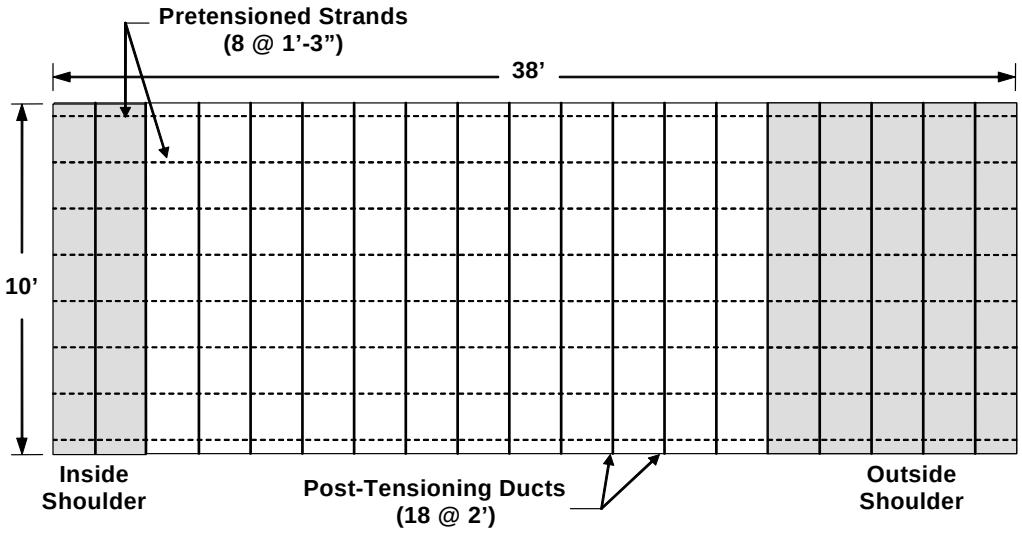

Figure 3.3 – Plan view of typical base panel

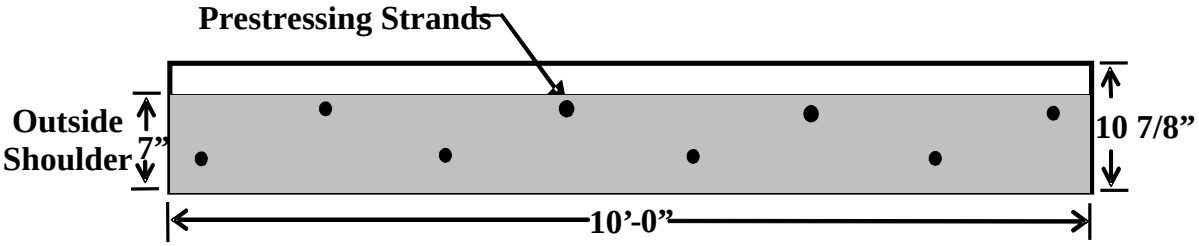

Figure 3.4 – Section of base panel looking perpendicular to traffic direction

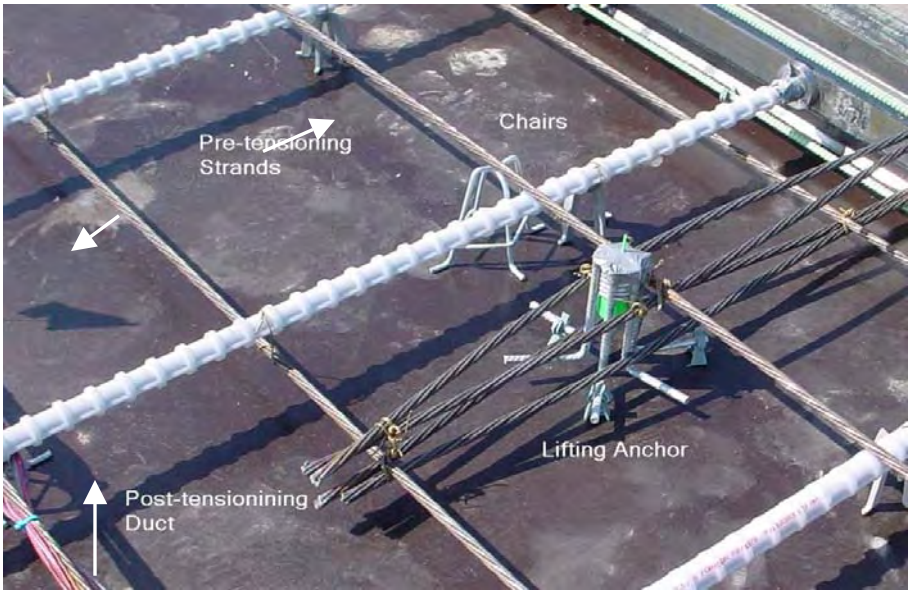

Figure 3.5 –Lifting anchor, chairs, and prestressing strands

3.2.1.2. ANCHOR PANELS

Anchor panels are essentially base panels with full depth holes near the center. These panels are located in the center of each PPCP section and anchor the entire section globally providing for equal expansion and contraction on either side of the anchor panels. Dowels were driven into at least 2' into the base layers and sub grade through the 4 in (10.2 cm) blocked-out anchor sleeves (see Figure 3.7). They were then grouted, anchoring the entire section. Figure 3.6 shows a plan view of a typical anchor panel. These panels required very little extra labor; therefore, they were cast intermittently with base panels.

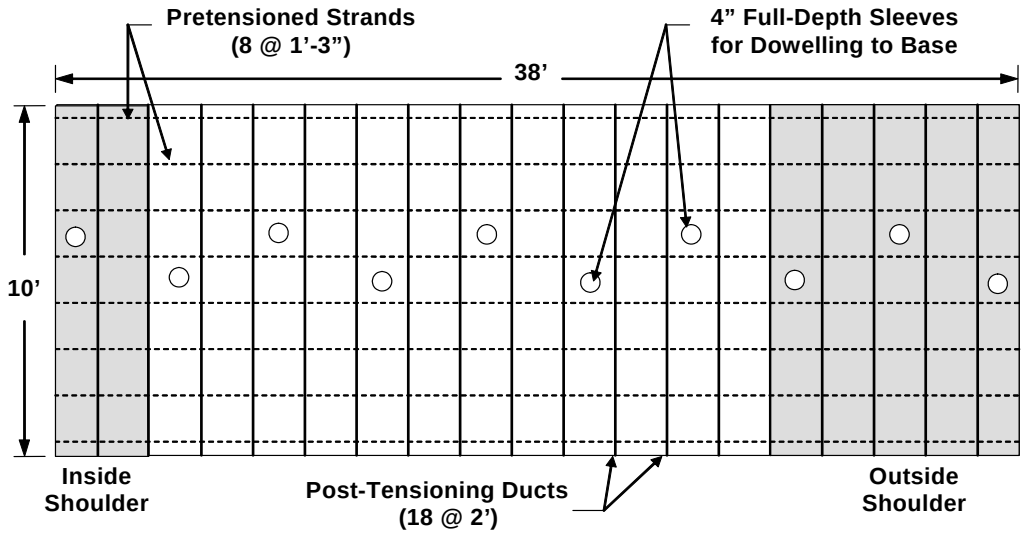

Figure 3.6 – Plan view of typical anchor panel

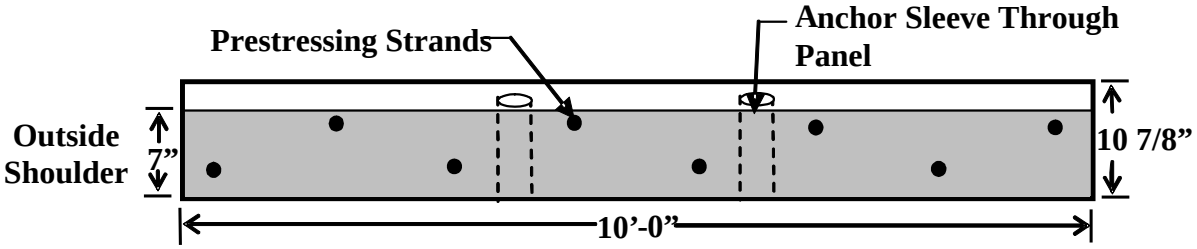

Figure 3.7 – Section of anchor panel looking perpendicular to traffic direction

3.2.1.3. JOINT PANELS

Joint panel fabrication began mid-December. Due to the complexities of retooling, amount of reinforcement, and nature of the panel itself, each joint panel had to be cast in two separate halves.

Figure 3.8 shows a plan view of a typical joint panel. Block-outs toward the center of the panel allow access to the post-tensioning ducts. These were filled during the final stages of construction. Joint panels have 12 pre-tension strands instead of 8 (see Figure 3.9). The top strands are draped with the slope of the crown (see Figure 3.5). Each half is connected by smooth dowels that provide load transfer between sections (not

shown in schematic). These dowels had to be held in place during casting. There also had to be some type of bond-breaker or cold-joint between sections to allow the joint panel to open up during post-tensioning operations. Therefore, a bulkhead was placed in the middle of the bed in order to cast each half separately. Figure 3.10 shows two halves of a joint panel, one side is cured, the other is ready for casting. Five joint panels were fabricated in all. Two of the five are located on the ends of the PPCP section as a transition from/to conventional pavement to PPCP pavement and were not cast with post-tensioning block-outs on one side (this side was simply dowelled into conventional cast in place concrete). Two joint panels were fabricated every two days.

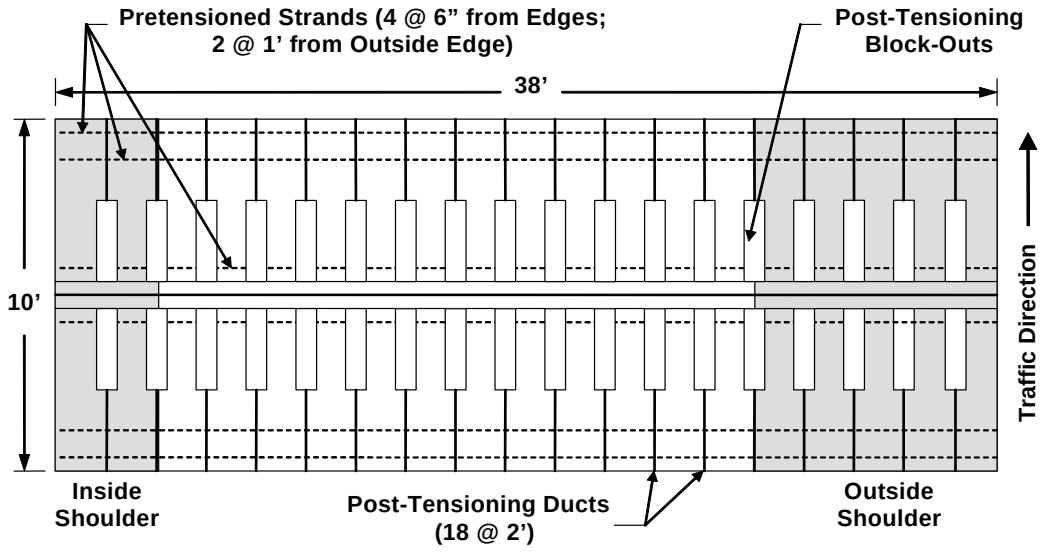

Figure 3.8 – Plan view of typical joint panel

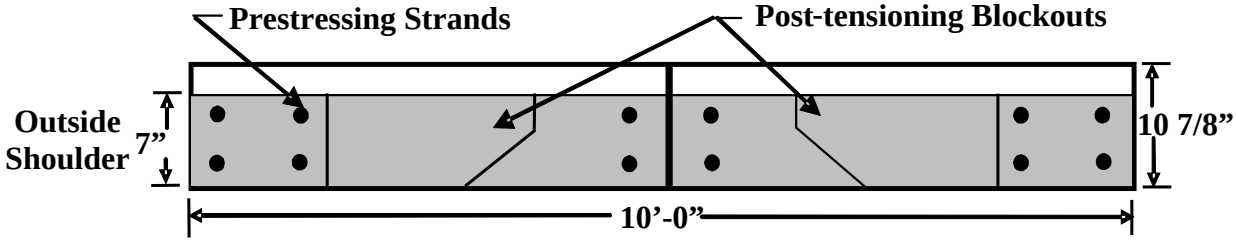

Figure 3.9 – Section of joint panel looking perpendicular to traffic direction

Figure 3.10 - Joint panel casting (left side cured, right side ready for casting)

3.2.2. SPECIFICATIONS

Dimensional and material specifications were developed before casting. Visual inspection and formwork measurements were completed by MoDOT personnel before each panel was poured. CPI designed the mix used for constructing the PPCP system and tailored it to meet MoDOT specifications. The tolerances for formwork were generally 1/8" (3.2mm). Pre-tensioning strands were 7 wire 0.5" diameter strands with 270 ksi (1860 MPa) ultimate strength (ASTM A416). Initial jacking force was 75% of ultimate (0.75 * 270 ksi = 202.5 ksi; 202.5 ksi * 0.153 in^2 = 31 kips [138kN]). Horizontal and vertical tolerances of post-tensioning ducts were within 0.25" (6.4mm) with the ends being 0.125" (3.2mm).

Details of the mix design are summarized in Table 3.1. The water content reported is the total water content including moisture present in the aggregates. The coarse and fine aggregate weights are for aggregates in a saturated surface dry (SSD)

moisture state. The mix was designed for a release strength of 3,500 psi (24 MPa) (with steam curing over-night) and 28 day strength of 5,500 psi (38 MPa) (500 psi higher than specified by MoDOT). The minimum specified air-entrainment was 5%, and the maximum specified slump was 6 in. Internal concrete temperatures had to be at least 16 °C (60 °F) in order to cast.

The Type I Portland cement was purchased from Buzzi Unicem in Festus Missouri. The fine aggregate was Crowley's Ridge Sand from Razor Rock in Harrisburg, AR, and the coarse aggregate was MoDOT #7 Salem Limestone from Vulcan Materials – Reed Quarry in Grand Rivers, KY. Admixtures used were manufactured by Degussa Admixtures, Inc. The admixtures include MB-AE 90, an air-entraining agent, Glenium 3000 NS, a full-range water-reducer, and Pozzolith 200 N, a water-reducer (Degussa 2006). The water used was Memphis municipal potable water. It was heated on very cold days to keep the concrete warm enough for casting.

Table 3.1 – CPI Mix design used in PPCP system

Constituent	Precast Pavement Mix
Cement	722 lb/yd^3
Fine Aggregate	1162 lb/yd^3
Coarse Aggregate	1766 lb/yd^3
Water	28.25 gal
Water - Cement Ratio	0.326
Air Entrainment Admixture	MB AE 90 1 -3 oz / yd^3
Full-Range Water-Reducer	Glenium 3000NS 4 - 8 oz / 100 lb Cement
Water Reducing Admixture	Pozzolith 200N 2 -5 oz / 100 lb Cement

Male and female shear keys were cast into opposite sides of each panel, regardless of panel type as can be seen in Figure 3.11. Shear keys were only provided in the traffic lane part of the cross-section (i.e. no shear keys along the inside and outside shoulders.) This provides for vertical load transfer between panels during in-service as well as lines them up during assembly. Panels were not match cast, rather the interchangeable panels were produced using intricate formwork and careful quality control.

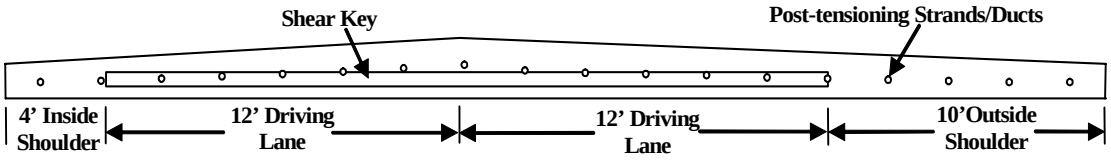

Figure 3.11 – Typical panel section looking with the direction of traffic

3.2.3. MANUFACTURING PROCEDURES

Panels were cast two at a time on an elevated steel bed. The precast bed used is considered 'self-stressing' in that the initial stress from the strands is transferred into the bed itself (along the entire length) and not resisted by large bulk-heads (Figure 3.12). Typical day to day operations were as follows:

1. **5:00 am – 8:00 am**: Strength tested on previous day's panel, steam is shut off, tarp removed, formwork loosened, pre-tensioning strands cut, panel removed from bed and stacked
2. **8:00 am – 1:00 pm**: Formwork tightened, bed oiled, strands run, strands stressed, ductwork placed, outside rebar placed
3. **1:00 pm – 5:00 pm**: Concrete air and slump tested, panels poured, vibrated and consolidated, hand screed, vibratory screed, hand trowel, broom finished, covered, let concrete sit, began fabricating ductwork for following day, turned steam on before leaving
4. **5:00 pm – 5:00 am**: Steam cured panels

Figure 3.12 - Casting bed showing tensioned strands and bulkheads

3.2.3.1. CASTING & FORMWORK

The steel forms, after removing the two panels from the night before, are shown in Figure 3.13. If strength was sufficient, panels were typically removed by 8:00 am and the re-tooling process started shortly thereafter. Figure 3.14 shows stressing operations being monitored by Terry Fields senior MoDOT inspector. Terry measured the formwork each morning and monitored stressing and placement to ensure quality control. Figure 3.15 shows a CPI worker installing a white polypropylene post-tensioning duct. A slender steel bar was temporarily placed in each duct to provide rigidity and prevent sag. Figure 3.16 shows placement and consolidation of concrete in a typical base panel. Besides inserting steel bars, wooden spacers shown were notched to fit over the ductwork and hold it in place during consolidation. Standard pencil type electric vibrators were used for consolidation. Figure 3.17 and Figure 3.18 show the screeding and finish work. A broom finish was used to provide temporary texture prior to the driving lanes being diamond ground after placement for smoothness requirements.

Figure 3.13 – Freshly oiled casting beds are inspected every day

Figure 3.14 – Applying pre-stressing force to strands of two panels

Figure 3.15 – Installing post-tensioning ductwork through pre-tensioned strands

Figure 3.16 – Placing and consolidating concrete on a typical base panel

Figure 3.17 – Hand leveling concrete of one panel just after placement

Figure 3.18 – Screeding and hand-finishing before final broom

3.2.3.2. STEAM CURING OPERATION

Steam curing was used in order to obtain adequate strength so that the pre-tensioning could be performed the following morning and allow for quick turn around on the molds. Plastic tarp was draped over the panels immediately after hand finishing was performed. Steam temperatures were recorded for several panels.

3.2.3.3. PRE-TENSION TRANSFER

Pre-tensioning transfer is a critical stage of fabrication in the life of precast panels. The concrete must be strong enough at a young age to withstand the compressive load transferred after cutting the pre-tensioning strands. Strength testing of concrete cylinders was completed prior to stress transfer to ensure that the concrete met specified strength at transfer. If the target strength, 3500 psi (28 MPa), was not reached then the de-molding operations were delayed and another test performed a few hours later. When the target release strength was reached, two workers cut the pre-tensioning strands via torches at the same time at each end of the panel. By alternating the strand cutting from the left and right side of the centroidal axis, eccentric loading on the panels was minimized.

Figure 3.19 - Releasing the Pre-tension force

3.3. CONSTRUCTION

Gaines Construction from Wentzville, MO was hired to construct the PPCP section. Construction speed was limited by available delivery trucks. Panel placement rates varied between 8 and 25 panels/day. The following sections describe the final construction of the PPCP system on I-57 near Charleston, MO.

3.3.1. BASE PREPARATION

Base preparation is one of the most important steps in construction of PPCP systems. Voids beneath the panels can cause improper alignment or added stress on shear keys. Friction between the panel and the base itself must also be mitigated. Frictional restraint can cause residual tensile stresses and reduce the life of the pavement (Merritt, McCullough et al. 2002).

Cast-in-place pavement fills uneven voids in the base and creates a smooth driving surface, whereas PPCP must bridge the voids in the base in order to have a smooth riding surface. Therefore, it is desirable to get a consistently level base before placement of PPCP.

For the Missouri project, the contractor chose a 4" asphalt treated base over permeable 4" crushed stone filter layer. A treated base is gap-graded and has a very low percentage of fine aggregates. It allows water to pass through freely to nearby edge drains. Asphalt leveling courses are a good choice for base because they can be placed both quickly and economically and still retain strict tolerances such that voids beneath the precast will be minimal (Merritt, McCullough et al. 2002). It should be noted, however, that mobilization of asphalt paving equipment to place a short section of leveling course makes it less economical (Merritt, McCullough et al. 2002). The Missouri project was

long enough to justify the asphalt treated permeable base. Figure 3.20 shows a joint panel over asphalt base on I-57.

Figure 3.20 – Joint panel on polypropylene over asphalt, and aggregate base (Missouri project) (Note: Instrumentation data cable exiting the end of the panel)

3.3.2. FRICTION REDUCTION LAYER

Long sections of PPCP will expand and contract with daily and seasonal temperature variations. Frictional restraint can cause tensile stresses and allow cracks to propagate, reducing design life. As stated earlier, this is more critical during decreases in temperature because as the slab contracts frictional forces will cause tensile strains. Conversely, expansion will create compressive strain which is not as significant of concern because concrete is typically strong in compression.

One way to reduce pavement friction is through the use of a single layer of polyethylene sheeting (Merritt, McCullough et al. 2002). Figure 3.20 (above) shows the polypropylene sheeting.

3.3.3. JOINT SEALANT

A slow curing two part epoxy type joint compound was used on all of the panel joints during placement. This sealed the joints to prevent water migration and pumping. It also provided lubrication between panels, making alignment much easier. Joint compound was typically applied while the panel was on the truck or just after unloading. Figure 3.21 shows application of joint compound on the female shear key of a joint panel.

Figure 3.21 – Application of joint compound to a PPCP panel

3.3.4. PLACEMENT OF PANELS

Alignment quickly became an important process. Panels were taken directly from trucks and placed with the adjoining section (Figure 3.22). Each was set, aligned, and two 0.6 in (1.5 cm) diameter post-tensioning strands were fed through. These strands were stressed (at low stress levels) to recover slack and gaps in the section. Not only did the individual panel alignment matter, but global alignment relative to the end of the

section was very critical. The following actions outline the steps taken to ensure alignment:

1. The centerline of the PPCP section was surveyed and nails were driven into the asphalt treated base several feet apart down the centerline.
2. Local panel-to-panel alignment was done with a standard contractor's laser. This laser was surveyed and aligned with the centerline (the nails).
3. The centerline of the panel was marked with a PVC pipe stuck into the center post-tensioning duct. When the laser hit the PVC squarely, the center of the panel was in the center of the road.

Global alignment took precedent over panel-panel alignment. Therefore, post-tensioning strands became difficult to thread.

Figure 3.22 – Unloading panel for placement

3.3.5. POST-TENSIONING

Once the laborious task of threading eighteen 250 ft long strands through each of the four sections was complete, stressing operations commenced. Each post-tensioning strand is 0.6 in diameter with 270 ksi ultimate strength. They were stressed to 80% of

ultimate (about 44 kips or 196 kN each). See Figure 3.11 for a distribution of post-tensioning strands. Gaines stressed two strands at a time working from the inside out (see Chapter 8 for specific order) to eliminate eccentricities. Figure 3.23 shows the simultaneous stressing operations of two post-tensioning strands. The jacking force was re-applied at the opposite end to ensure uniform stress distribution.

Figure 3.23 – Stressing the second set of strands in a typical Missouri PPCP section

3.3.6. GROUTING & FINISHING

The last step in the Missouri PPCP construction process is to grout the tendons and fill the block-outs. Grouting provides an extra layer of corrosion protection for the post-tensioning tendons. The PVC duct is not continuous across the joints, therefore, water and chlorides may come in contact with post-tensioning strands (the joint sealer prevents this). Fully bonded tendons will also allow damaged sections to be cut out and replaced if needed sometime in the future without losing post-tension stress in the remaining section.

Grout was pumped into vents located at several panels. Figure 3.29 shows two small grout vents just above the repaired crack. Once grouting was finished the entire driving surface was diamond ground to eliminate roughness from elevation differences between panels.

3.3.7. UNFORESEEN CHALLENGES DURING CONSTRUCTION

The problem that was most taxing on completion time was threading the post-tensioning strands. Each section had at least two strands run one panel at a time. The other sixteen were threaded through the panels for the full 250 feet. Poor alignment, sagging ducts, and ice were suspected impediments to the strand threading process. Gaines used several techniques to thread the strands. The first was a strand pusher (see Figure 3.24). This mechanical pusher proved moderately effective. The most innovative method was removal of the king wire from a 250 ft seven wire strand. This king strand was welded onto the end of a full strand, shown in Figure 3.25, and pulled through with a back-hoe.

Figure 3.24 – Post-tensioning strand pusher

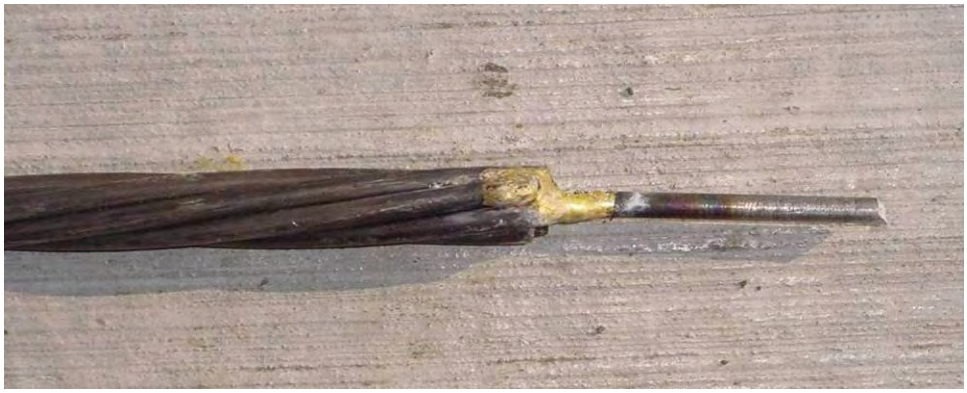

Figure 3.25 – King strand welded to full strand for threading

The epoxy which was used to lubricate the panels during placement was allowed to harden due to delays in threading the post-tensioning strands. With hardened epoxy between panels, uniform load transfer between panels was hindered and post-tensioning behavior was altered from stressing 25 – 10’ panels to stressing a monolithic 250’ section.

Another issue that impeded the construction process was that mistakes in alignment were cumulative with respect to the length of the road, seen in Figure 3.26. Correction of misaligned panels proved to be a difficult problem because the post-tensioning ducts only permitted small changes in orientation or else the strands could not be fed through. To solve this problem, Gaines used wooden and steel shims on the south side of several panels to realign the pavement in order to meet the existing pavement at the far end. A close view of these shims can be seen in Figure 3.27.

Figure 3.26 – Crooked PPCP section (before and after shimming started)

Figure 3.27 – Shim installed on the outside shoulder of several panels

Another issue that held up construction was when the joint panels did not open up after stressing. Ideally the joints would have opened during stressing, allowing the installation of expansion material. To aid in opening the joints by jacking, the tops of the joints were saw-cut in order to create stress concentrations on the bonded portions, which is shown in Figure 3.28. The joints were pulled apart and expansion material was finally

installed as required. One expansion joint between section 3 and 4 did not open properly and cracked a couple inches from the joint. More on this cracked expansion joint is discussed later in the report.

Figure 3.28 – Closed joint in joint panel after stressing operations (saw-cut on top)

Some panels displayed transverse and longitudinal cracking. These cracks became evident in both the casting yard and construction site. Cracks were filled with an epoxy type sealant to prevent freeze-thaw damage and chloride ingress, Figure 3.29.

Figure 3.29 – Repaired transverse crack in PPCP

4. EXPERIMENTAL PROGRAM

4.1. LABORATORY MEASUREMENTS

The following sections describe the laboratory experiments that were conducted on the concrete used in the precast pavement project. Specimens were cast alongside the panels and subjected to the same steam curing environment. Tests were performed to establish mechanical properties of the concrete so as to facilitate analysis and evaluation of service performance.

4.1.1. COMPRESSIVE STRENGTH TESTS

The compressive strength of each specimen set was determined at 7, 28, and 56 days of moist curing. The tests were performed in accordance with ASTM C-39, "The Standard Test Method for Compressive Strength of Cylindrical Concrete Specimens" (ASTM 2005). The 6" x 12" cylindrical specimens were first capped to ensure parallel and smooth ends using Gilson Rediron 9000 sulfur mortar capping compound. This procedure was performed in accordance with ASTM C-617, "Standard Practice for Capping Cylindrical Concrete Specimen" (ASTM 1996). A Forney 600 kip capacity concrete compression testing machine pictured in Figure 4.1 was used for the actual compression tests. Specimens were loaded at a rate of 45-50 psi/s in accordance with ASTM C-39. The compressive force was measured on the hydraulic line with a pressure transducer. Three LVDT's evenly distributed around the specimen with an 8" gage length measured strain. Load output from the testing machine and displacement output

from the three LVDT's were recorded using a National Instruments data acquisition (DAQ) card and LabVIEW.

Figure 4.1 – Compression test setup for capped 6" diameter cylinders using 3 LVDT's and a Forney Compression Machine

4.1.2. UNRESTRAINED CREEP & SHRINKAGE

Specimens for creep and shrinkage were prepared in the same manner as the cylinders used the strength tests. Shrinkage tests were started after the specimens had cured for one day. Creep tests were started on the 28th day. An overview of the specimen preparation process is reviewed in the following section followed by details of shrinkage and creep tests respectively.

4.1.2.1. SPECIMEN PREPARATION

Five creep and five shrinkage specimens were cast during instrumentation trips to the precasting yard. Only four of the five specimens cast were used in the actual tests. Two of the specimens were sealed (at 100% relative humidity) and two of the specimens

were unsealed and subjected to 50% relative humidity for unrestrained creep and shrinkage studies. A very specific process was used to prepare the specimens for the subsequent tests. This process is outlined below in detail and has been proven effective in previous research projects at the University of Missouri – Columbia (Earney 2006).

4.1.2.1.1. MOLD PREPARATION

Prior to casting, the 6" x 12" cylinder molds were prepared. The molds meet the requirements of ASTM C 470/C 470M-02a, "Specification for Molds for Forming Concrete Test Cylinders Vertically." Figure 4.2 is a photograph of a typical mold used. The molds contained three sets of equidistant holes to accommodate anchors for attaching extensometers. Temporary spacer bars to fix the distance between anchors were manufactured. The steel spacer bars measured 12" x 1" x 1/8" with two holes drilled 10" apart. Brass anchors on the interior of the mold were attached to the spacer bars with greased machine screws.

Figure 4.2 – Interior and exterior view of cylinder molds used for creep and shrinkage. Brass anchors and spacer bars are seen (Earney 2006)

4.1.2.1.2. CASTING AND CURING

All specimens were cast in accordance with ASTM C31/C31M-03A, "Standard Practice for Making and Curing Concrete Test Specimens in the Field." Five specimens used for shrinkage were cast October 12, 2005, and five specimens for creep were cast on December 9, 2005. Casting of the cylinders along with precast panels is shown in Figure 4.3. Both the creep and shrinkage specimens were steam cured with the precast panels to ensure the samples were representative of the concrete in the pavement panels.

The specimens used for shrinkage were immediately transported back to the laboratory the next day and the molds removed to begin testing. The creep specimens were placed in a moist curing room until an age of 28 days. To accommodate free shrinkage the spacer bars in both specimen types were removed within 8 to 24 hours of casting.

Figure 4.3 – Creep and shrinkage cylinder casting during instrumentation trips to the precast yard

4.1.2.1.3. CAPPING AND SEALING

Prior to capping and sealing all specimens were de-molded by drilling a small hole in the bottom of the mold and using compressed air to remove the plastic mold. Loose debris and moisture on the ends of the cylinders was removed by blowing compressed air over the specimens.

The four cylinders were capped in the same fashion as the compression specimens to ensure parallel ends. Two each of the capped creep and shrinkage specimens were sealed using aluminum foil tape. Studies done in the lab have proven the combination of sulfur mortar capping compound on either end and aluminum foil tape wrapped around specimen prevents over 99% of moisture losses. Figure 4.4 shows capped and sealed specimens ready for extensometer attachment.

Figure 4.4 – Picture of capped and sealed specimens used for creep and shrinkage studies (Earney 2006)

4.1.2.1.4. EXTENSOMETER ATTACHMENT

Brass anchor sets cast 120^{o} apart around the circumference of the cylinders secured shrink wrapped studs to the specimens. The studs were screwed into the

specimens after curing and upon completion of capping and sealing. The heat shrink was needed to electrically isolate the extensometers and provide a grip. Extensometers with a 10” gage length were then affixed between the three sets of studs. A close-up view of the stud and extensometer connection is seen in Figure 4.5. A zip tie properly positioned was used to secure the extensometer to the stud. All extensometers were manufactured at the University of Missouri – Columbia and individually tested and calibrated (Earney 2006).

Figure 4.5 – Close-up view of extensometer attachment to stud screwed into brass insert cast in concrete cylinder (Earney 2006)

4.1.2.2. CREEP SPECIMEN LOADING AND INSTALLATION

Four creep specimens were loaded into the creep frame shown in Figure 4.6 at an age of 28 days. Prior to loading, the procedure outlined in the previous section regarding specimen preparation was followed. The capped specimens with attached extensometers were stacked in the creep frame. A hydraulic jack was then placed between two steel plates at the top of the frame and a load was applied. The frame was located in a sealed chamber to hold the temperature and relative humidity constant. Details of this

humidity/temperature controlled curing chamber are discussed further in the section on Test Control and Data Acquisition.

Figure 4.6 – Creep load frame with two sealed and unsealed specimens loaded in compression (Earney 2006)

4.1.2.2.1. DETAILS ON CREEP FRAMES

Creep frames are required to apply a constant load and measure the creep strain history of concrete. Spring loaded creep frames designed and implemented on a previous research project at the University of Missouri – Columbia were used for this test (Eatherton 1999). Springs apply constant load when compressed to prescribed levels, which is a very important characteristic for monitoring creep. The support structure of the frames consists of three vertical steel columns. At the top of the frame there are two steel plates. These plates are used to house a hydraulic jack that applies the initial stress to the concrete specimens. When the jack has compressed the cylinders to a desired load mechanically, the nuts above the bottom steel plate are secured in place to retain the

sustained compression load. A load cell under the bottom plate was used to monitor load for the duration of the experiment. The load cell was calibrated to measure the load of the jack by using strain gages that are glued to the inside of the cell. Below the load cell there is a small concrete stub cylinder used to distribute end restraint stresses. The stub cylinders also ensure that load is applied to the test cylinders through a "poisson ratio" compatible load pattern. Underneath the stub cylinder are the four test cylinders (two sealed and two unsealed). Between each cylinder is a pair of Teflon sheets to reduce friction between capped cylinders. The bottom of the creep frame includes another concrete stub cylinder. The cylinders rest on a circular steel plate that is rotationally unrestrained due to its spherical seating. The three springs at the bottom of the frame maintain the prescribed constant load applied via the hydraulic jack (Eatherton 1999).

4.1.2.3. SHRINKAGE SPECIMEN INSTALLATION

A total of four shrinkage specimens were monitored. Two were sealed and two were unsealed. After specimen preparation described earlier, the cylinders were placed in a hermetically sealed chamber and hooked up for continuous monitoring. A sealed specimen placed in the chamber with extensometers attached is shown in Figure 4.7. Monitoring began at an age of one day and continued until 83 days. The specimens were carefully placed in the sealed chamber such that they would not be disturbed during the entire duration of the experiment.

Figure 4.7 – Sealed shrinkage specimen with three extensometers attached for measurement of shrinkage strains (Earney 2006)

4.1.2.4. TEST CONTROL AND DATA ACQUISITION

Sophisticated data acquisition techniques and environmental controls have been developed and are used for many of the previous mentioned laboratory experiments. The following sections summarize these aspects of the program.

4.1.2.4.1. AUTOMATED TEMPERATURE AND HUMIDITY CONTROLLED CHAMBER

A hermetically sealed chamber constructed at the University of Missouri – Columbia maintained the unrestrained creep and shrinkage specimens at a constant relative humidity of 50% (± 1%) and ambient temperature of 24^{o}C (± 0.5 ^{o}C). The atmosphere of the chamber was digitally controlled using a custom developed LabVIEW program. The front panel displayed in Figure 4.8 shows a time history of relative humidity and temperature. Preset upper and lower limits of relative humidity and temperature were used to determine when devices needed to be activated to modify conditions within the chamber. The automated program could also be switched and controlled by the user.

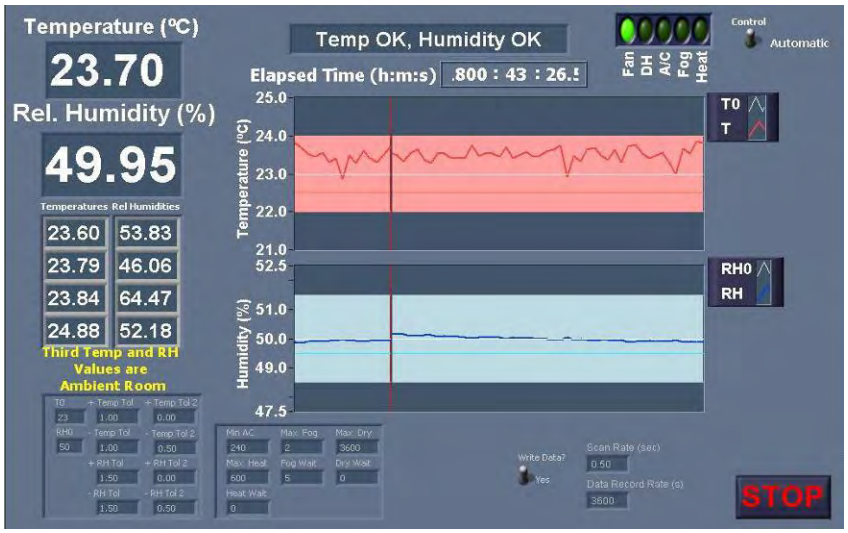

Figure 4.8 – Front panel view of LabVIEW control program for hermetically sealed chamber where creep and shrinkage specimens are located during testing (Earney 2006)

4.1.2.4.2. LABVIEW PROGRAMS FOR DATA ACQUISITION

Strain and load measurements were acquired via a LabVIEW program. For each individual specimen the program recorded elapsed time, the strain in each of the three extensometers, and the output from the load cell for creep specimens. Data acquired during monitoring was saved to a file that could be imported into Microsoft Excel. Calibration factors were applied during data manipulation where averaging techniques were used to minimize the number of data points (Earney 2006).

4.1.3. CHLORIDE PERMEABILITY TESTS

All chloride penetration tests in this study were conducted according to ASTM C-1202 or AASHTO T-277, "The Standard Test Method for Electrical Indication of Concrete's Ability to Resist Chloride Ion Penetration" (ASTM 2005). All of the equipment and setup to complete this test was designed and constructed according to the standard.

4.1.3.1. TEST SETUP

The test setup shown in Figure 4.9 was constructed at the University of Missouri – Columbia for a previous project (Stundebech, 2007) and is in accordance with the two standards mentioned earlier. The system is designed to test up to 12 specimens at any given time. Individual specimens are connected to a regulated 60 V DC power supply and current measuring system. The voltage regulators used are accurate to ±0.1V.

A computer automated data acquisition (DAQ) system was used to collect data, and consisted of a National Instruments DAQ card and LabVIEW software. The LabVIEW program acquired data points of current and time every 5 seconds. The data points were averaged and written to a spreadsheet file every 10 minutes for the duration of the 6-hour test.

Upon completion of the 6-hour test the total charge passed (or area under the time-current plot) was calculated using the trapezoidal rule. Table 4.1 provides a basis for determining the chloride ion penetrability of concrete specimens and as recommended in the ASTM standard.

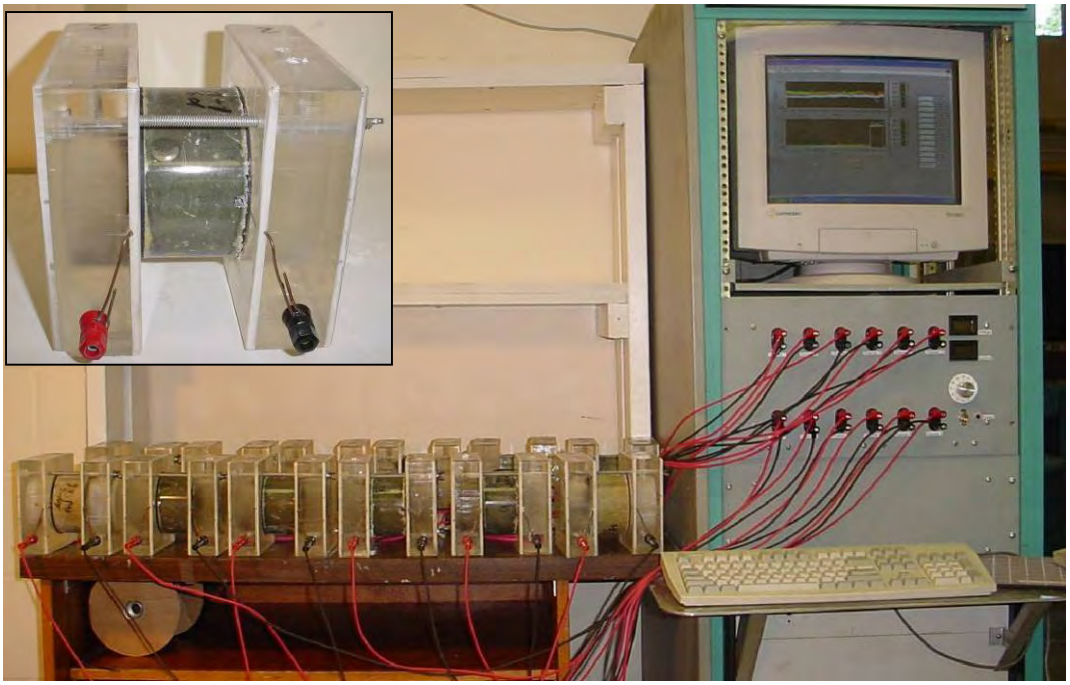

Figure 4.9 – Rapid chloride penetration test setup (Stundebech 2007)

Table 4.1 – ASTM designation for chloride ion penetrability based on charge passed (ASTM 2005)

Charge Passed (Coulombs)	Chloride Ion Penetrability
>4,000	High
2,000-4,000	Moderate
1,000-2,000	Low
100-1,000	Very Low
<100	Negligible

4.1.3.2. SPECIMEN CONDITIONING

Preparing specimens for the test was a multi-step process. Two days prior to the 6-hour chloride ion penetration test, 4" diameter cylinders were removed from the moist curing room, de-molded, and the sides were generously coated with a two-part epoxy

from PolyCarb to seal them. The two part epoxy was allowed to cure overnight, and three specimens were cut from each cylinder. A diagram of the specimen geometries and where the cylinder was cut is shown in Figure 4.10.

The next step in the specimen conditioning process involved de-airing. The specimens were placed in the conditioning chamber depicted in Figure 4.11 and vacuum desiccated for three hours. De-aired water was then drawn into the bucket until the specimens were completely submerged. Vacuuming continued for one-hour, and then air was allowed to reenter the chamber. The specimens continued soaking in the bucket for 18 ± 2 hr before the actual test commenced.

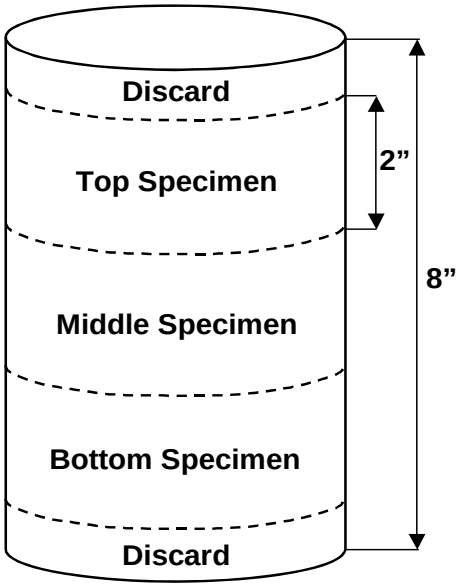

Figure 4.10 – Diagram of specimen slicing to be used for the rapid chloride penetration test

Figure 4.11 – Photograph of the rapid chloride penetration test specimen conditioning equipment

4.1.3.3. PROCEDURE

The conditioned specimens were removed from the conditioning equipment and towel dried. The specimens were placed in the cells shown in Figure 4.9, and two rubber gaskets were placed on either end of the specimen before bolting the cells together. The side of the specimen hooked up to the positive terminal was filled with 0.3N NaOH, and the negative side was filled with 3.0% NaCl solution. The electrical leads were then plugged in after verifying the voltage across the leads was 60 V. The automated data acquisition system described earlier was used to collect data from the six hour test.

4.1.4. FREEZE-THAW TESTING

The freeze-thaw tests were conducted according to Procedure A of ASTM C-666, "The Standard Test Method for Resistance of Concrete to Rapid Freezing and Thawing" (ASTM 2003). ASTM C-215, "Standard Test Method for Fundamental Transverse,

Longitudinal and Torsional Resonant Frequencies of Concrete Specimens," was used to determine the dynamic modulus of the concrete specimens (ASTM 2002). Four of the six prism specimens that were cast were subjected to the rapid freezing and thawing test.

4.1.4.1. TEST SETUP

The freeze-thaw chamber at the University of Missouri – Columbia is capable of subjecting 18 prisms to approximately 10 freeze-thaw cycles every 24 hours. A single cooling unit freezes the specimens and strip heaters between the specimens thaw the concrete. The chamber is controlled by a concrete prism with two embedded thermocouples. One of the embedded thermocouples is connected to a chart recorder to monitor the number of cycles, and the other is connected to a control circuit that switches the heaters and cooling unit on and off. In Figure 4.12 freeze-thaw specimens are seen in the chamber. The specimens are placed in stainless steel containers allowing for a minimum of 1/8" of water to completely surround the concrete specimens.

Figure 4.12 – Overhead view of cabinet used to subject prisms to freeze-thaw cycles

4.1.4.2. PROCEDURE

The prism specimens cast were steam cured with the pavement panels at the precasting yard, and then transported to the University of Missouri – Columbia and moist cured until an age of 28 days. The specimens were removed from the curing room and placed in the freeze-thaw chamber and brought to a temperature of 40^{o}F. Initial readings of weight and fundamental transverse frequency were then taken. After these initial readings the specimens were subjected to approximately 30 freeze-thaw cycles in between measurements of weight and fundamental transverse frequency. A total of 300 cycles is required to complete the test.

The fundamental transverse frequency of the concrete specimens was measured with the test-setup shown in Figure 4.13, according ASTM C-215. An electromechanical driving unit oscillates the specimen at frequencies varied by the user. A lightweight pickup unit at the opposite end of the specimen measures frequency. An oscilloscope on the control unit indicates when the end of the specimen and the pickup needle are in phase (the driving frequency is varied to accomplish this). Being in phase established the first fundamental transverse frequency.

The relative dynamic modulus of the specimens were then calculated and plotted against time to determine the damage done to the concrete from rapid freezing and thawing. The relative dynamic modulus is simply the ratio of the dynamic modulus after the specimen is subjected to a number of freeze-thaw cycles to the dynamic modulus of the virgin specimen. This ratio when reported as % is also called the durability factor. Concrete subjected to 300 freeze-thaw cycles that has durability exceeding 60% is considered acceptable.

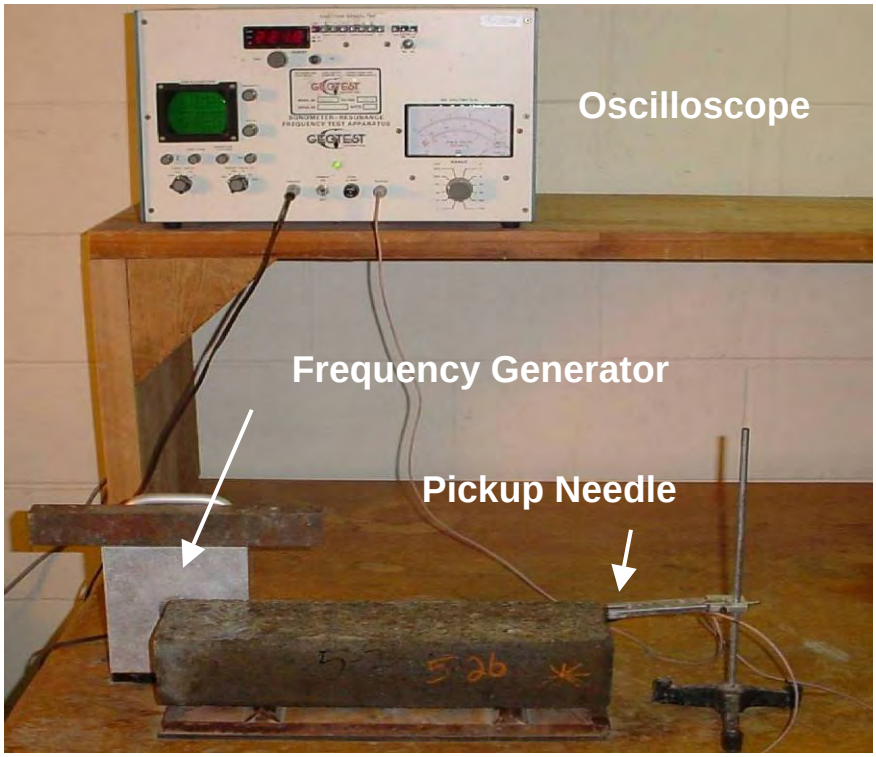

Figure 4.13 – Frequency generator and setup for measuring fundamental transverse frequency

4.1.5. FLEXURE TESTS

Flexure tests were performed in accordance with ASTM C 78, "Standard Test Method for Flexural Strength of Concrete" (Using Simple Beam with Third-Point Loading)" (ASTM 2002).

4.1.5.1. TEST SETUP

The test setup used at the University of Missouri – Columbia is shown in Figure 4.14. The apparatus subjects concrete specimens to third point bending and measures gross and net deflections of the beam with two LVDT's. The LVDT on the bottom of the specimen measures the gross deflection, which takes into account both beam deflection and local crushing of the concrete at the supports. The LVDT labeled "Net" in Figure 4.15 only measures the deflection of the beam relative to the ends. An MTS machine

with closed loop control and 110 kip capacity was used to deflect the beam. A computer based DAQ using a National Instruments DAQ card and LabVIEW program collected both deflection measurements from the LVDT's along with the applied load.

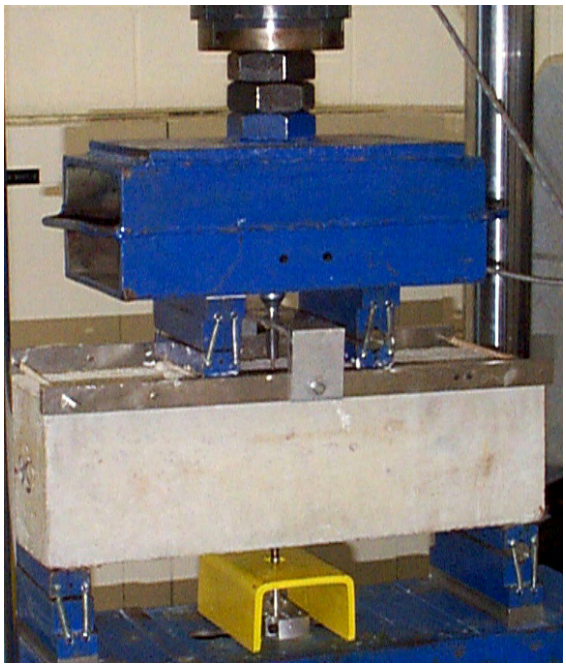

Figure 4.14 – Photograph of third point loading of concrete prism/beam

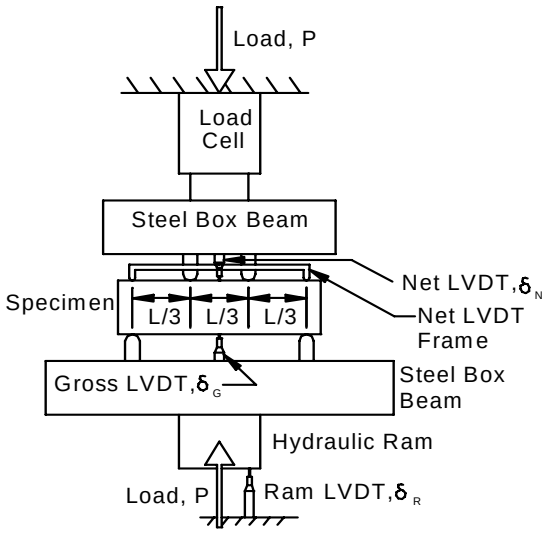

Figure 4.15 – Details of test setup used to test flexural strength of concrete specimens

4.1.5.2. PROCEDURE

The prism specimens were cast along with the precast panels at the precasting yard and allowed to steam cure with the panels. The molds were then transported back to the moist curing room at the University of Missouri – Columbia. When ready for testing the specimens were removed from the curing room and de-molded. The rectangular beam specimens were placed sideways on the bottom steel box beam. The "Net LVDT Frame" depicted in Figure 4.15 was secured with plaster of paris on either end, and a small preload is applied to remove any slack in the testing apparatus. The flexural test was conducted under specimen displacement control by a ramp loading function until flexural failure. Values calculated at the conclusion the experiment include; the modulus of rupture (f_r), the Young's modulus (E_c), the total energy absorbed, and the fracture energy (G_f).

4.2. FIELD MEASUREMENTS

The MU Research Team made two separate trips to instrument the seven designated panels at CPI in Memphis, TN. The first trip took place during the week of October 10, 2005. Four designated base panels (Panels B1-4) and anchor Panel (C1) were instrumented. During the second trip, the week of December 4, 2005, the two remaining joint panels were instrumented.

The MU research team spent the early morning hours each day installing the instrumentation. Instrumentation was tested on-site prior to concrete placement to ensure all systems were working properly. Pre-tensioning took place around 8:00 AM each day. The forms were assembled and prepared for concrete placement. The research team

worked closely with CPI employees to avoid interfering with the casting process. The instrument locations were then flagged to ensure they were not damaged by personnel during panel fabrication. Initial values were recorded before casting to obtain baseline references for each gage. Casting began at 2:00 PM, and steam was turned on at approximately 5:00 PM every day. Readings were recorded all night during hydration curing until prestress transfer the next morning.

Details of the test section are presented, followed by specific instrumentation locations within the instrumented panels in the next few sub-sections. A look at the five strain and temperature measuring devices used for observation and their function, and an overview of the data acquisition system are also presented. More details on the instrumentation are included in Dailey (2006) and Davis (2006).

4.2.1. INSTRUMENTATION LABELING

The precast panels used in the project are identified by two different methods. The identification system used by CPI and Gaines Construction used letters and numbers to signify the different panel types. An "A" panel was a joint panel, a "B" panel was a base panel, and a "C" panel was an anchor panel. Since three different types of joint panels were used, a number after the "A" differentiated the joint panels. Labels "A1" and "A2" represented the joint panels at the north and south limits of the overall pavement test section respectively. The symbol "A3" was used for the three intermediate joint panels in the project.

To differentiate the instrumented panels from the non-instrumented panels the MU research team added a number after the symbols used by the contractors. The panel numbering increased from south to north. For example the four base panels were labeled

B1, B2, B3 and B4. The southern-most base panel was B1 and the northern-most was B4. The single instrumented anchor panel was marked C1, and the joint panels were marked A31 and A32 respectively.

The gages within the panels were further identified by their type and location. Vibrating wire gages were marked with a V, instrumented rebar with an R, thermocouples with a T, and strandmeters with an S. The location of the gage was identified by a number after the type of gage.

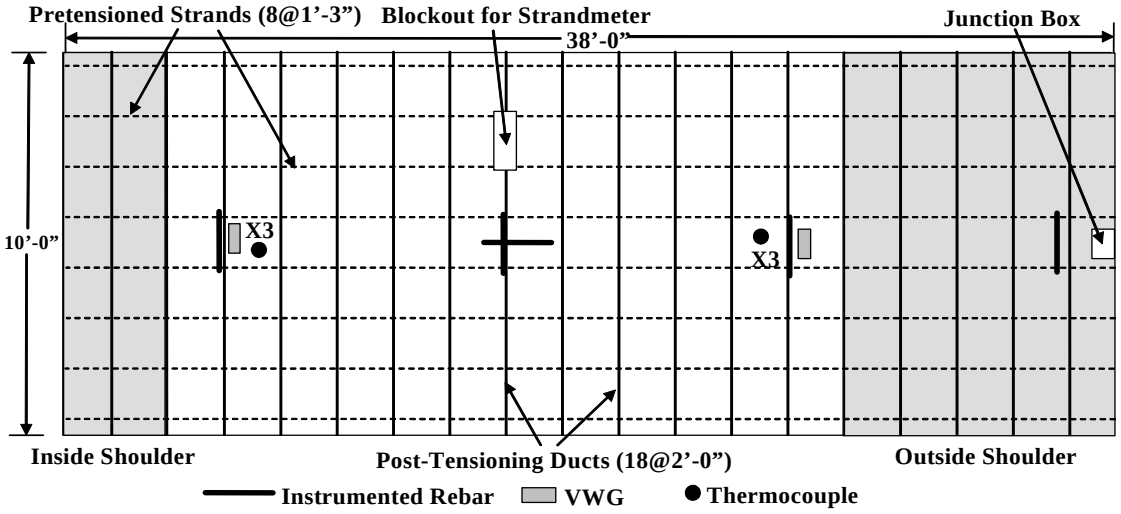

Figure 4.16 – Typical instrumented base or anchor panel

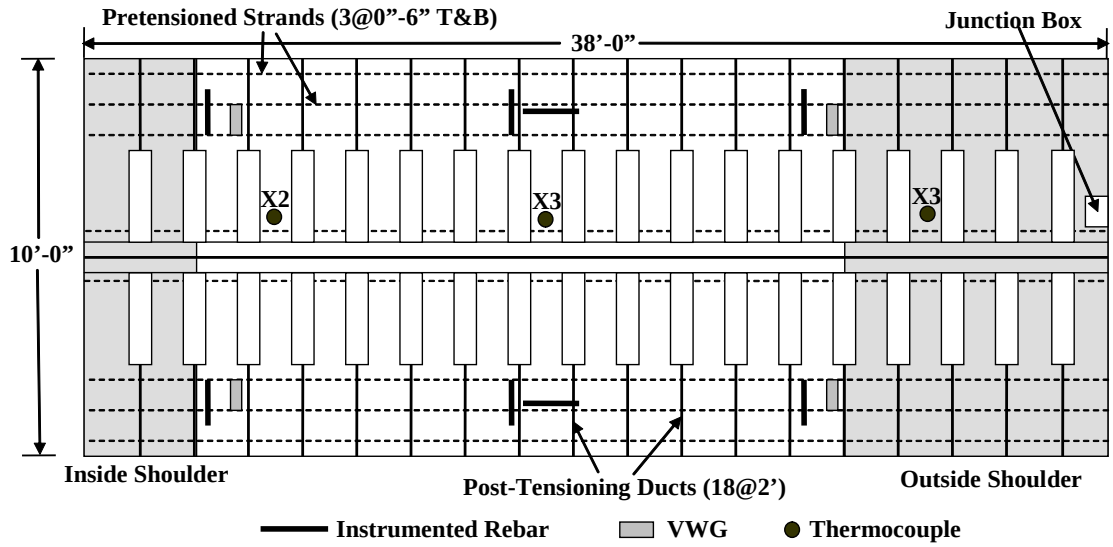

Figure 4.17 – Instrumented joint panel A32

4.2.2. INSTRUMENTATION LOCATIONS

The pilot project encompassed 1,010 feet of roadway rehabilitation and consisted of four, 250' long post-tensioned sections. The primary goal of the research program was evaluate the performance of the PPCP with regard to temperature, loading, local strains, and joint displacements. To accomplish this, the research team decided to focus on a single 250' section and instrument panels within this section. Section 3 of the 4 sections along the traffic direction was chosen. It was selected based on its proximity to an AC power source and to limit possible transition effects from conventional concrete pavements adjacent to the PPCP. Four base panels, two joint panels, and one anchor panel were instrumented to understand the characteristics of the individual panels and how they perform under service loads. Figure 4.18 shows the location of the instrumented panels within the chosen section. The panel marked B4 in Figure 4.18 lies outside the third section and was instrumented for redundancy purposes.

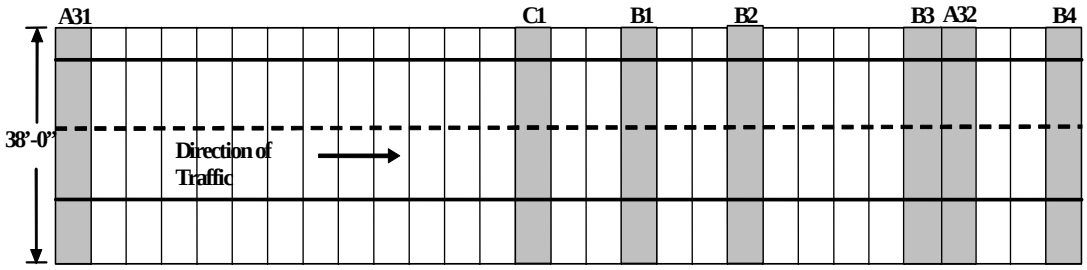

Figure 4.18 – Overall view of test-section and location of instrumented panels. (A refers to a joint panel, B refers to a base panel, and C refers to a anchor panel)

4.2.2.1. INSTRUMENTED PANELS

The seven instrumented panels incorporated five different devices to measure strain and temperature of the concrete along with strain in the post-tensioning strands. Figure 4.16 depicts typical instrumentation in a base or anchor panel and Figure 4.17 shows the instrumentation locations in joint panel A32. Concrete strain was measured using instrumented rebar and vibrating wire gages and strain in the post-tensioning strands was measured by vibrating wire strandmeters. Temperature measurements were observed by thermocouples and iButtons (Maxim) embedded in the concrete along with thermistors incorporated in the vibrating wire gages.

4.2.3. TYPES OF INSTRUMENTATION

4.2.3.1. STRAIN GAGE REBAR

Four standard 20', #4 (nominal diameter = 0.5"), Grade 60 rebar sections were used to fabricate the strain gage rebar for the project. The 20 foot rebar sections were cut into ten equal sections nominally measuring 24 inches in length. Both ends of the 24 inch section were machined smooth and threaded to accommodate for gripping during

calibration. A full strain gage bridge was installed on each 24 inch rebar section. Gages were chosen with backings that matched steel's thermal behavior. A schematic of the strain gage configuration is shown in Figure 4.19 below. The two-inch machined section was degreased, sanded smooth, and cleansed before strain gage application. Two gages were installed transverse to the length of the rebar and the other two were installed along or longitudinal to the length of the rebar with cyanoacrylate glue. The ribs on either side of the rebar were used to line up the gages consistently. After gage application, wires were run to complete the bridge. By using a full bridge of active strain gages, thermal effects on measured strains are eliminated.

A completed strain gage rebar is shown in Figure 4.20. Strain gage instrumented rebars are capable of measuring very dynamic events such as stress transfer from strand cutting and traffic loads while in-service. The instruments are also very robust and have a good track record from previous projects completed here at the University of Missouri – Columbia (Eatherton 1999).

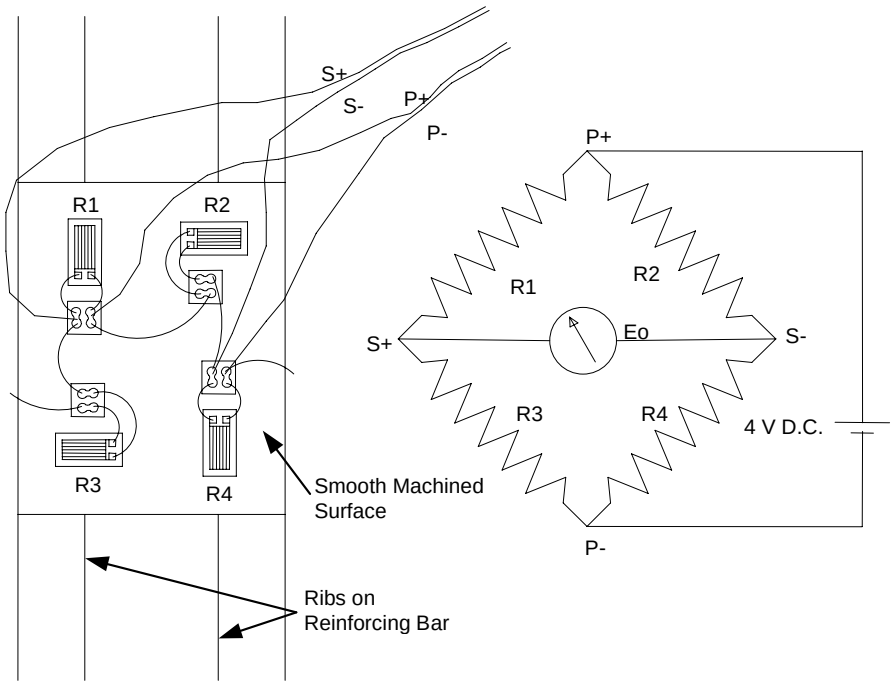

Figure 4.19 – Schematic of the strain gage configuration on the strain gage rebar (Eatherton 1999)

Figure 4.20 – A completed strain-gage bar along with an instrumented bar yet to be waterproofed and sealed (Eatherton 1999)

4.2.3.2. VIBRATING WIRE STRAIN GAGES

Model 4200 Vibrating Wire embedment type strain gages were used (Geokon Inc.). The 6 inch gage is depicted in Figure 4.21. The gage consists of a wire stretched between two flanges, an electromagnetic plucking device, and a thermistor used for temperature measurement. The gage operation relies on the change in resonant frequency

of the wire based on its length. When one flange displaces relative to the other, the wire is elongated resulting in a change in resonant frequency. This change in resonant frequency can then be related to strain by simple mechanics.

The vibrating wire gages are very useful for long-term strain measurements; however, dynamic events cannot be measured due to settling time of the transducer. The unstrained initial reading of the gage serves as the baseline for long-term strain measurements . At any time the zero reading can be referenced, and the state of strain of the concrete can be determined.

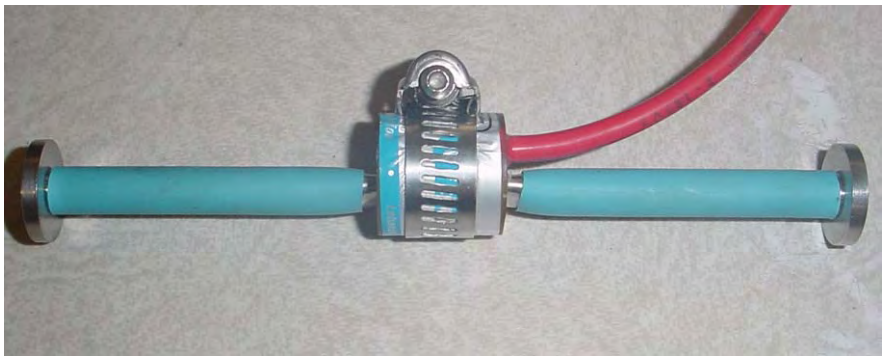

Figure 4.21 – Model 4200 vibrating wire gage from Geokon Incorporated

4.2.3.3. VIBRATING WIRE STRANDMETERS

Model 4410 Vibrating Wire strandmeters were also purchased from Geokon Incorporated and is shown in Figure 4.22. The gage operates on the same principles as the model 4200 discussed previously. However, clamps at either end accommodate fixing the transducer to prestressing strands. Individual calibration information was supplied by Geokon. They were additionally calibrated by the research team along with the support instrumentation used with these transducers.

The main purpose of the gage was to measure strain with prestressing strands at various times. Calculation of frictional losses associated with strand stressing and time-

dependent prestress loss due to creep, shrinkage and relaxation can be completed. The gages were encased in a PVC tube filled with grease in order isolate the gage from the surrounding concrete and only measure strain in the post-tensioning strand.

Figure 4.22 – Model 4410 vibrating wire strandmeter purchased from Geokon Incorporated

4.2.3.4. THERMOCOUPLES

Type T thermocouples utilizing a copper-constantan junction were used for concrete temperature measurement. The specified temperature range was -328^{o} to 663^{o} F (-200° to 900° C). The thermocouples were cut to length, welded using thermocouple welders, and coated in epoxy at the University of Missouri – Columbia. This type of temperature measuring device is very advantageous due to its robustness, ease of use, and accuracy (+/- 0.1^{o} C).

4.2.3.5. IBUTTONS

iButtons manufactured by Dallas Semiconductors were also used to measure temperature. Twelve Dallas Semiconductor model DS1922L iButtons were purchased from Embedded Data Systems. The DS1922L is capable of measuring temperatures in a range from -40 ^{o} C to 85 ^{o} C with a resolution of 0.0625 ^{o} C. The iButtons store time and

temperature logs in self contained memory unit and only require a single lead wire to communicate with a computer or other datalogging device. Lead wires were soldered on the iButtons at the University of Missouri – Columbia, and the devices were coated in epoxy to protect them from contact with other ferrous materials and harsh chemical environments inside of the wet concrete.

4.2.3.6. GAGE INSTALLATION

All instruments were tested at the University of Missouri before being installed in the precast panels. The gages were sorted according to the specific panel they were installed in and boxed in plastic totes for transportation to the precast yard. The lead wires were cut to specific lengths depending on their location within the panel, labeled accordingly, and the ends were tinned in the laboratory to streamline gage installation at the precast yard and connection at the construction site.

Figure 4.23 and Figure 4.24 show installed gages just prior to casting. The vibrating wire gages were attached or "piggy-backed" on the instrumented rebar. Wooden spacers were used to ensure the gages did not touch. The zip ties holding the vibrating wire gages in place were purposely left relatively loose to ensure proper performance of the vibrating wire gages. Thermocouples used are shown in Figure 4.23. The thermocouples were attached to fiberglass bars to ensure proper spacing and electrical isolation from other devices. To get a profile of temperatures, thermocouples were located at the top, middle, and bottom of the cross-section. Figure 4.25 shows instrumented rebar installed in the longitudinal and transverse directions. Strandmeters were installed in blockouts in the panels designed for this purpose. An installed strandmeter is shown in Figure 4.26. To isolate the strandmeters from the grout used to

fill in the blockouts a PVC tube was secured around the gage. This is shown in Figure 4.27.

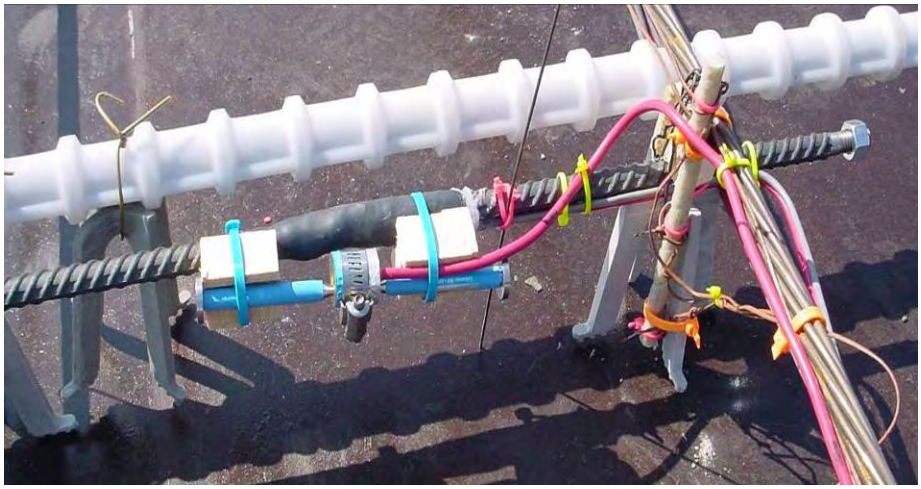

Figure 4.23 – Picture of installed gages just before casting of concrete

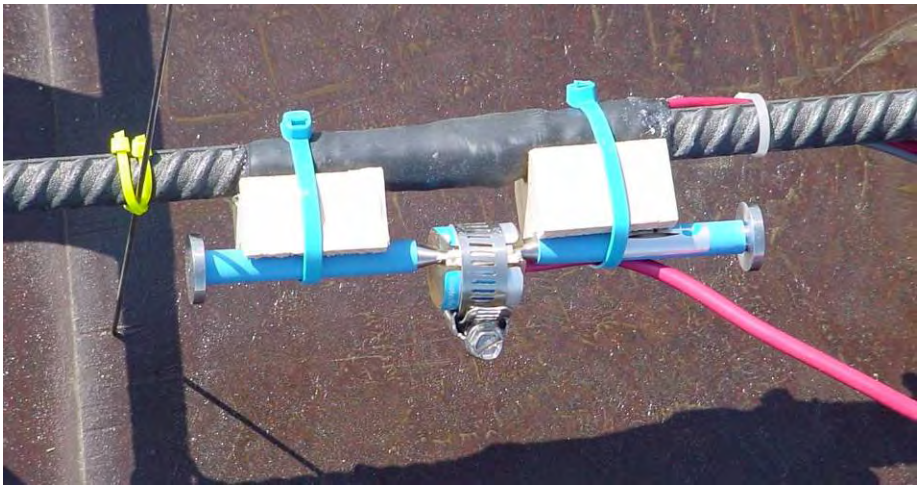

Figure 4.24 – Close-up view of vibrating wire gage "piggy backed" to instrumented rebar. Zip ties were relatively loose to ensure the gage was not bent

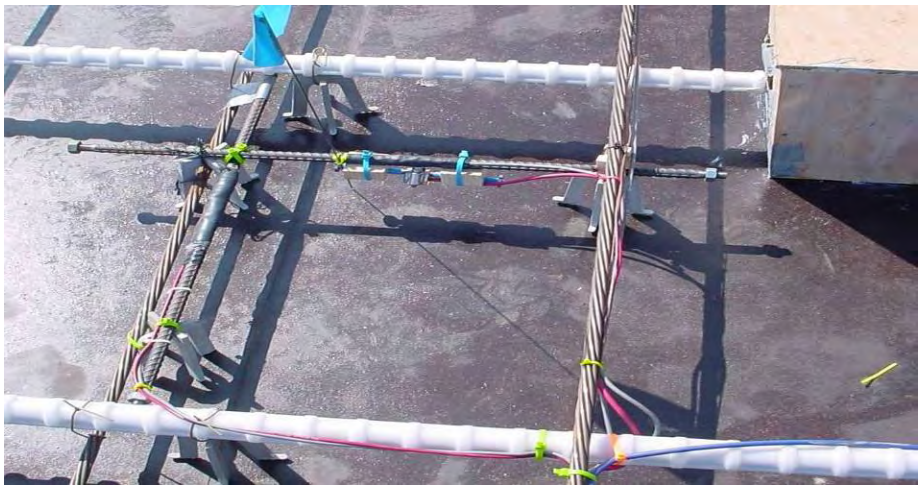

Figure 4.25 – Instrumented rebar installed longitudinal and transverse to the direction of traffic

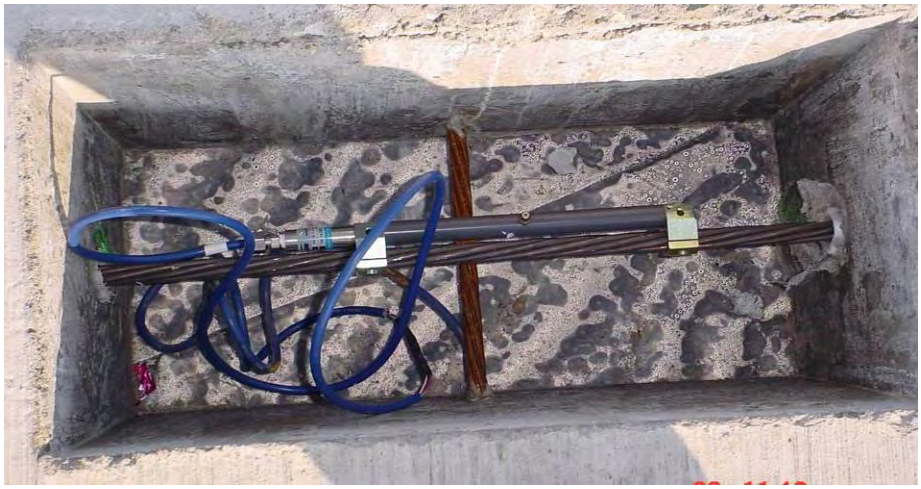

Figure 4.26 – Strandmeter installed inside blockout around post-tensioning strand. (Note: Rusty pre-tension strand in the transverse direction)

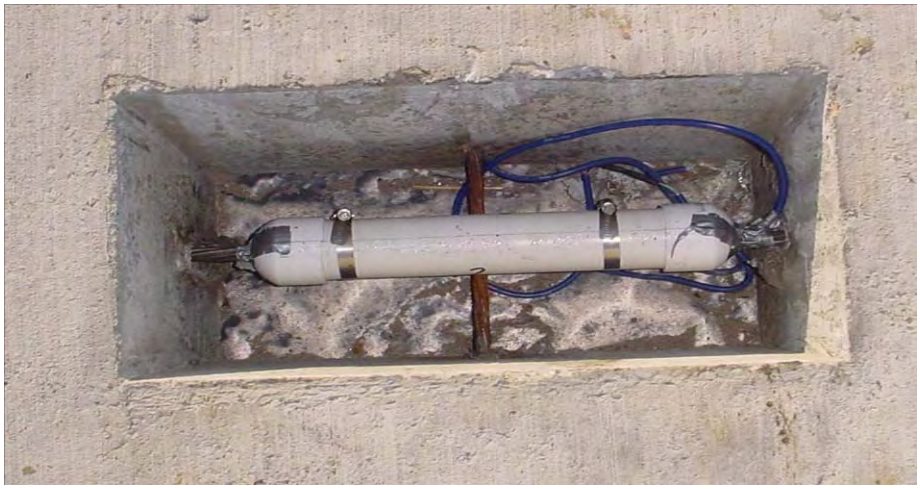

Figure 4.27 – Strandmeter encased in PVC tube to isolate it from grout

4.2.4. DATA ACQUISITION SYSTEM

The many capabilities of the data acquisition system are briefly discussed in this section. An in-depth discussion involving the data acquisition system is presented in "Instrumentation and Early Performance of an Innovative Prestressed Precast Pavement System" (Dailey 2006).

All instrumentation lead wires were run to blockouts cast in the outside shoulder of the precast panels. The junction boxes, shown in Figure 4.28, were fabricated at the University of Missouri – Columbia to accommodate quick connection, cold-junction compensation for thermocouples, and voltage step-down/regulation for the instrumented rebars. Multi-pair wires were run from the junction boxes to the data acquisition cabinet installed at the extents of the right of way for signal transmission. Figure 4.28 shows the signal cabinet and components of the main data acquisition system.

The cabinet is equipped with a 30 amp power supply and a DSL connection for remote communication. The Data acquisition system consists of a Campbell Scientific CR10X data logger, (3)-32 differential AM416 relay multiplexers, 110V AC to 12V DC power supply, two AVW1 vibrating wire interfaces, and an NL100 network link interface for remote communication. The remote communication feature allowed the research team to monitor real time performance of the pavement system and download/upload new programs as appropriate.

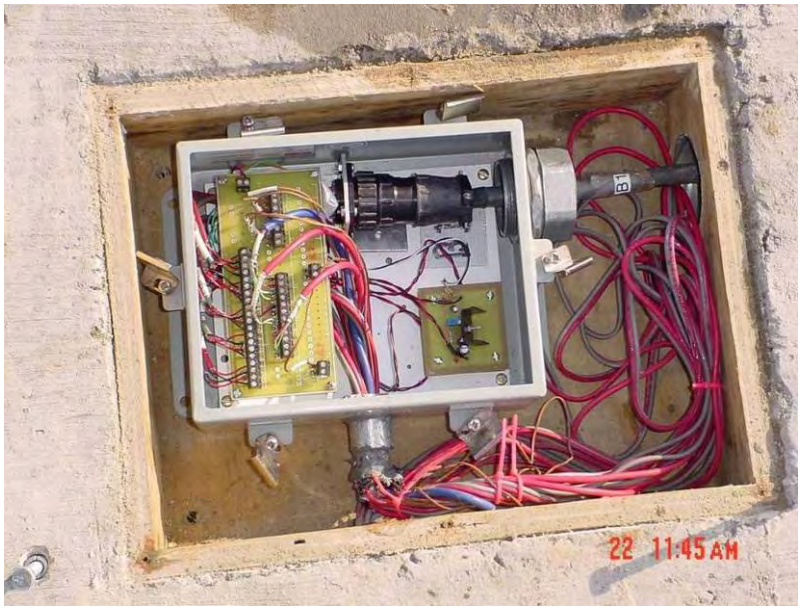

Figure 4.28 – Junction box installed in blockout cast in outside shoulder of precast pavement panels

Figure 4.29 – Signal cabinet with main data-acquisition equipment installed at the edge of right of way

5. CONSTITUTIVE MATERIAL PROPERTIES

5.1. RESULTS FROM LABORATORY MEASUREMENTS

Laboratory tests based on ASTM Standards were performed to determine mechanical properties of the concrete used for the pavement rehabilitation project. These properties include compressive strength and elastic modulus, unrestrained creep and shrinkage response, chloride permeability, freeze-thaw resistance, flexural strength and fracture energy for concrete. Manufacturers supplied properties were obtained for the prestressing strands and the conventional steel reinforcing bars.

5.2. MATERIAL PROPERTIES OF CONCRETE

5.2.1. COMPRESSIVE STRENGTH AND ELASTIC MODULUS

Compressive strength tests were performed on standard 6" diameter cylinders cast with each set of instrumented panels. Average results of strength and modulus of the specimens and comparisons to theoretical values are presented in Table 5.1. Early age modulus of elasticity measurements could not be recorded due to equipment malfunction. Concrete strength at an age of 7 days ranged from 5,210 psi (35.9 MPa) to 6,810 psi (46.9 MPa) with an average of 6,070 psi (41.9 MPa). At 28 days the strength ranged from 5,590 psi (38.5 MPa) to 8,700 psi (59.9 MPa) with an average of 7,190 psi (49.6 MPa), and at 56 days the strength range was 7,350 psi (50.7 MPa) to 9,960 psi (68.7 MPa) with an average of 8,830 psi (60.9 MPa). Modulus values at 28 days ranged from 5.22×10^6 psi (36 GPa) to 6.32×10^6 psi (44 GPa) with an average of 5.69×10^6 psi (39 GPa) and at 56 days the range was 5.45×10^6 psi (38 GPa) to 7.06×10^6 psi (49 GPa) with an average

of 6.26 x 10^6 psi (43 GPa). Average ultimate strain values at 28 days were 1,540 μstrain and at 56 days the average was 1,590 μstrain. The relatively high variation in compressive strength at various ages of the concrete may be attributed to varying amounts of admixtures contained in the two castings. As expected cylinders for each panel casting tended to have similar compressive strengths, but cylinders from different mixes at the same age varied in properties as described.

Prediction models of strength and modulus developed by (Branson et al) were used for comparisons to theoretical values. Figure 5.1 shows the strength versus time comparisons for the model and results from laboratory studies. The model used to predict strength accurately reflects measured results up to 28 days. Beyond 28 days the model under-predicted strength, and by an age of 56 days the difference was 15% less than experimentally measured strengths. Predicted modulus values were about 35% lower than measured values. A major factor that is not accounted for in the prediction models is the lower than normal water to cement ratios used in these particular concrete mixtures.

Figure 5.2 shows representative stress versus compressive strain results for two sets of castings at ages of 28 and 56 days. The figure demonstrates the increase in stiffness and strength of the concrete between the ages of 28 and 56 days. Strength increased 23% and the modulus increased 10% between 28 and 56 days.

Table 5.1 – Experimental averages and predicted results of concrete strength and modulus of elasticity at 7, 28, and, 56 days

Day	Experimental Strength		Predicted Strength		Experimental Modulus		Predicted Modulus	
	psi	MPa	psi	MPa	psi	GPa	psi	GPa
7	6,070	41.9	6,580	45.4				
28	7,190	49.6	7,290	50.3	5.69E+06	39.2	4.87E+06	33.6
56	8,830	60.9	7,430	51.2	6.26E+06	43.1	4.91E+06	33.9

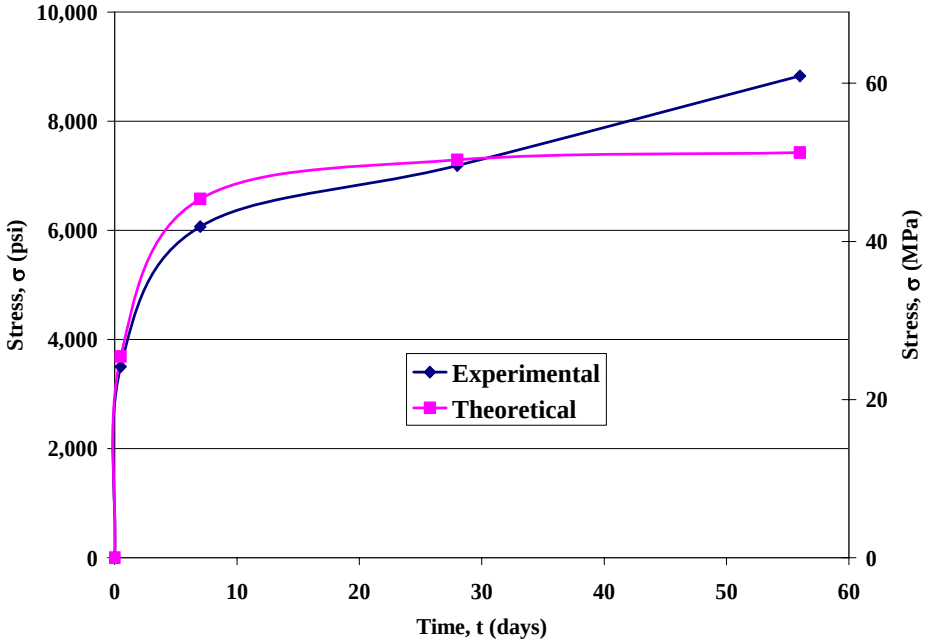

Figure 5.1 – Plot of experimental and theoretical strength versus concrete age

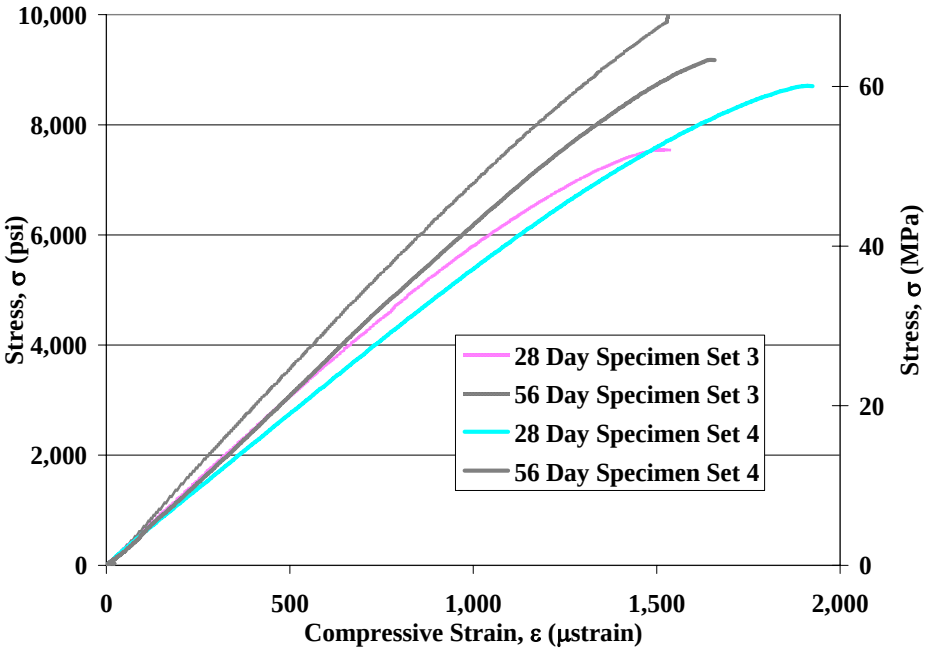

Figure 5.2 – Stress versus compressive strain results from 28, 56 day strength tests

5.2.2. UNRESTRAINED SHRINKAGE AND CREEP RESPONSE

5.2.2.1. Shrinkage Test Results

Typical results from the shrinkage tests and comparisons to theoretical values for unsealed and sealed specimens are presented in Figure 5.3 and Figure 5.4 respectively. Figure 5.5 shows the average results (three strain gages used for each cylinder) for sealed and unsealed specimens along with comparisons to theoretical values. For theoretical models it is assumed that the sealed specimen is subjected to 100% relative humidity conditions and the unsealed specimen is subjected to 50% relative humidity. The spikes in strain values in Figure 5.3 and especially in Figure 5.4 can be attributed to activities associated with instantaneous changes in humidity and temperature due to opening of the curing chamber for other experimental programs.

The sealed specimens exhibited 73% less shrinkage compared to the unsealed specimens. This difference implies that a large portion of the total shrinkage is due to drying shrinkage, which is a loss of moisture to the environment. The sealed specimens are assumed to be at 100% relative humidity. Therefore, the shrinkage observed in these specimens is mainly due to autogenous shrinkage, which is shrinkage associated with self desiccation.

The ACI prediction model for the unsealed specimen under-estimated strain results by 37% at 90 days. Early-age shrinkage results from the laboratory tended to increase much faster than compared to theoretical values. Beyond 28 days the change in magnitude of strains was similar for the laboratory results and the theoretical predictions. The smaller prediction by the ACI model at early ages (less than 28 days) is perhaps due to the high hygral gradient (50% relative humidity drying environment). The prediction

model for the sealed specimens tended to predict more accurately the results measured in the lab. The prediction model at 90 days was 20% less than the results from the laboratory. As seen in the unsealed specimens the early age shrinkage tended to be much higher in the laboratory as compared to the theoretical values.

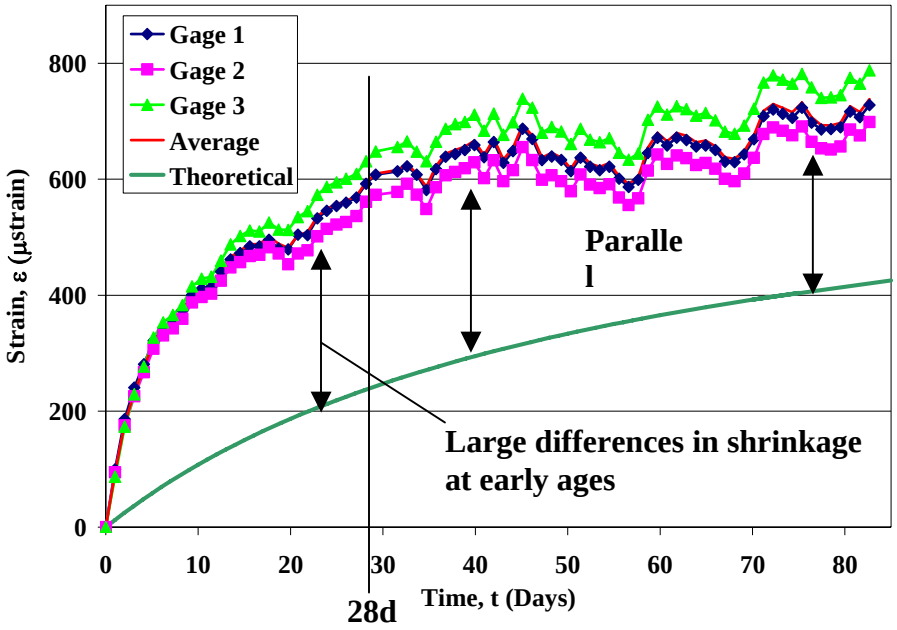

Figure 5.3 – Unsealed shrinkage specimen results along with ACI 209 prediction of shrinkage

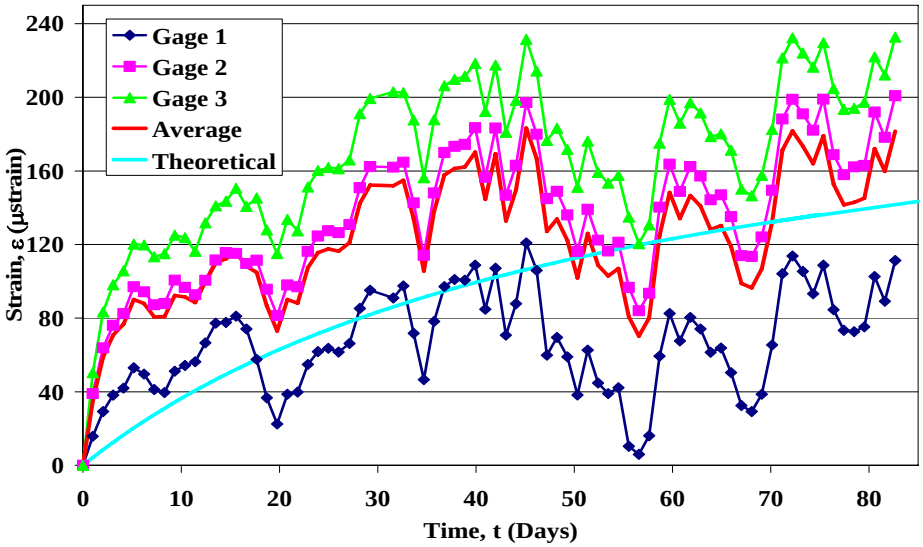

Figure 5.4 – Sealed shrinkage specimen and comparison to ACI 209 prediction of shrinkage

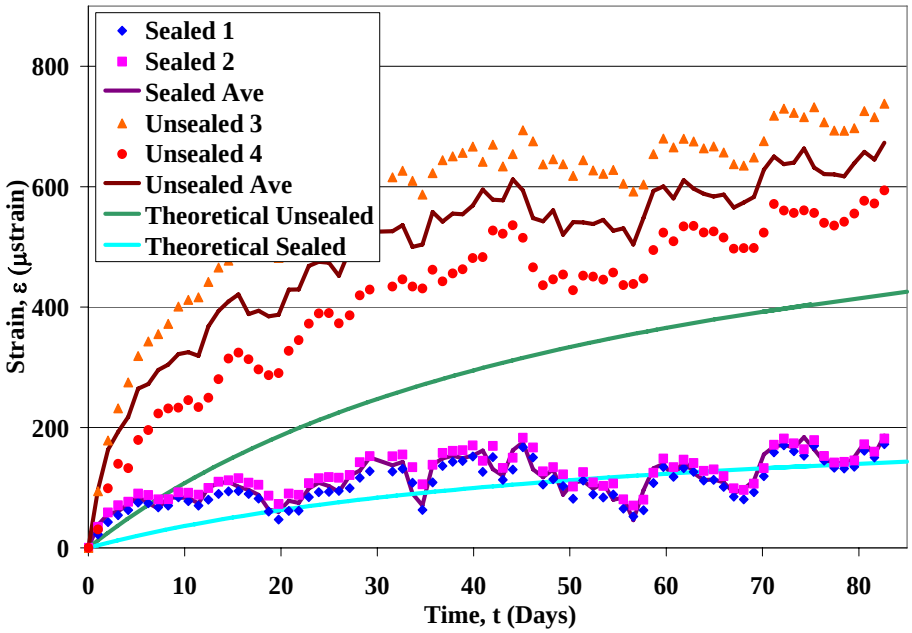

Figure 5.5 – Average values for two sealed and two unsealed shrinkage specimens and comparison with theoretical results

5.2.2.2. Creep Test Results

Four creep specimens were monitored for 60 days after initial moist curing for 28 days. Two of the specimens were sealed and two were unsealed. Theoretical values were calculated using prediction models published in ACI 209 (1997). The various correction factors calculated according to ACI 209 for the sealed and unsealed specimens are presented in Appendix B.

Theoretical predictions along with unsealed and sealed laboratory creep results are presented in Figure 5.6 and Figure 5.7 respectively. Average results (three strain gages used for each cylinder) from the creep specimens are shown in Figure 5.8. For theoretical models it assumed that the sealed specimen is subjected to 100% relative humidity conditions and the unsealed specimen is subjected to 50% relative humidity.

The initial elastic shortening of the cylinders (due to the 2,000 psi (14MPa) applied pressure) for both sealed and unsealed specimens averaged 350 μstrain. The

inherent modulus from this load and resultant displacement was 5.62 x 10^6 psi (39 GPA). This modulus value is within 1.5% of the value calculated from the compressive strength tests.

The predicted creep strains from the ACI 209 model closely resembled creep responses of the mix used for this project. The unsealed prediction model under-estimated measured creep strain by 10%, and the sealed prediction model under-estimated creep strain values by 5%. Creep coefficients were also calculated based on theoretical and measured results. For comparative purposes the creep coefficients were calculated at 60 days of sustained loading, and only the unsealed specimen's creep strains were used. The predicted creep coefficient was 1.66, and the measured creep coefficient was 1.82. This represents a 9.5% difference between the predicted and measured creep coefficient.

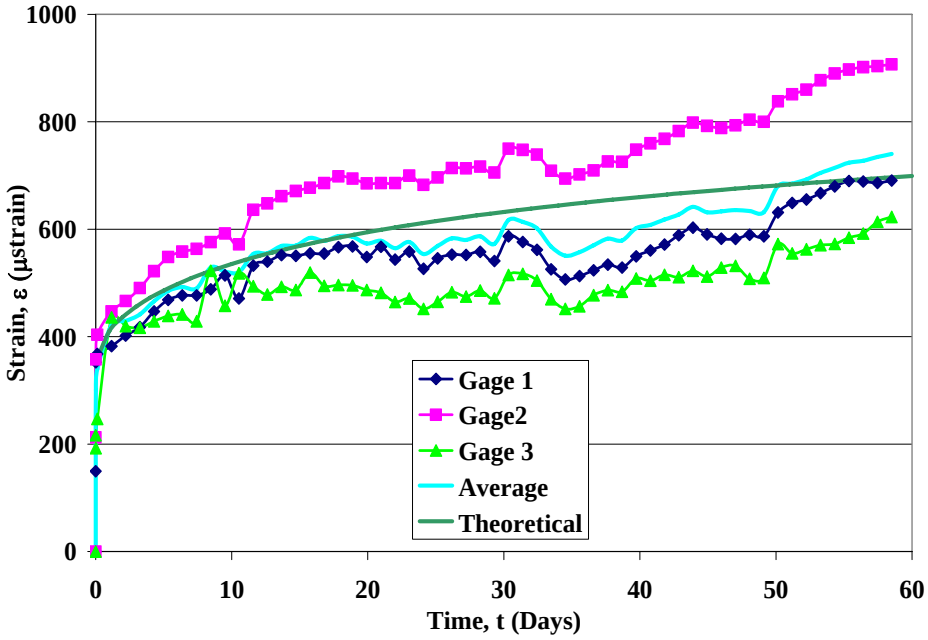

Figure 5.6 – Unsealed creep specimen and comparison to theoretical values calculated using ACI 209

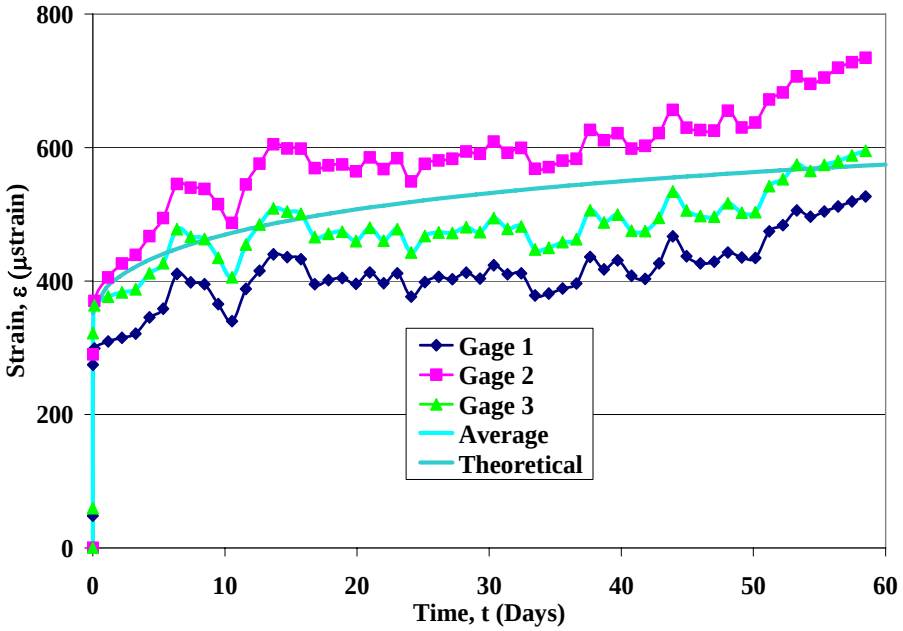

Figure 5.7 – Sealed creep specimen and comparison to theoretical values calculated using ACI 209

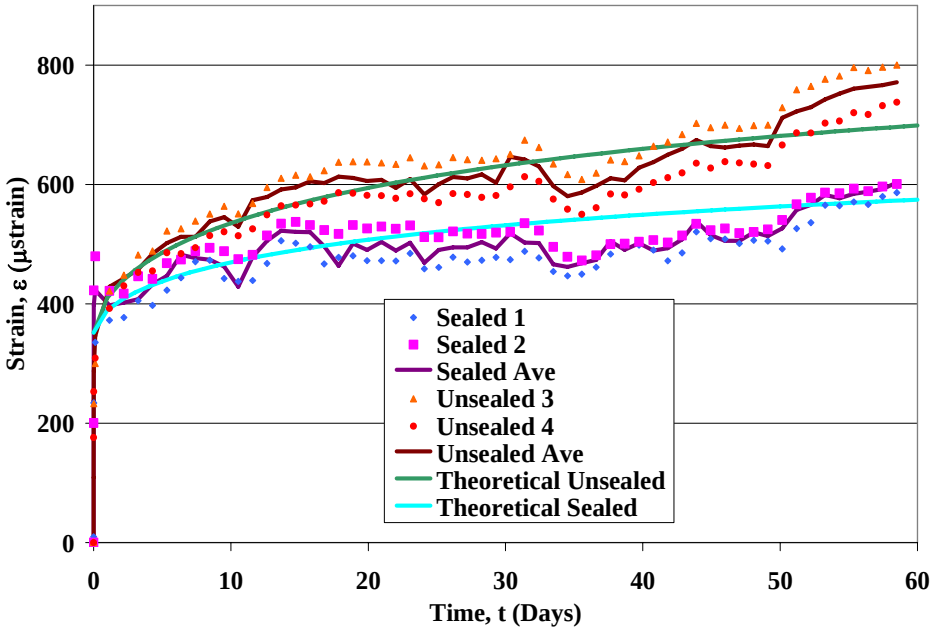

Figure 5.8 – Average creep values for two sealed and u two unsealed specimens along with comparison to ACI 209 models

5.2.3. CHLORIDE PERMEABILITY

Results from the rapid chloride permeability tests (RCPT) are presented in Table 5.2. Initially, only baseline readings at an age of 28 days were planned. However, because of the relatively high permeability readings recorded in these tests more specimens were cored from 6" diameter cylinders to repeat the test at an age of 112 days. Nine specimens were initially tested, and only four additional specimens could be cored due to a limited number of remaining specimens for tests at 112 days.

Table 5.1 presented earlier gives a baseline for quantifying results from RCPT. The average charge passed for the specimens at 28 days was 4,000 coulombs, which is high according to the guidelines set forth by ASTM. At 112 days the total charge passed decreased 22% to 3,150. This value is in the moderate range of chloride permeability according to ASTM standards. Literature reviewed (Stundebech 2007) also suggests looking at the first half-hour of the test and multiplying by twelve to obtain a more representative basis for comparison to other standard tests. Specimens tend to heat up as the test progresses which increases electron flow, thus resulting in over-estimation of chloride permeability (Hooton and Stanish 1997). From the data obtained the total charged passed based on the first half hour would be 3,160 coulombs and 2,430 coulombs for the 28 and 112 day tests respectively. These values represent more acceptable values according to the ASTM standard. In the literature review it was also discussed that the water to cement ratio plays a role on the influence of the accuracy of this test. The water cement ratios averaged around 0.33 for the pavement mix design, and it is stated in literature that the test is more accurate for values between 0.4 and 0.7 (Mindess, Young et al. 2003).

The 28-day readings for chloride permeability tended to be higher than expected, and the pavement should be monitored for possible chloride ingress in the future. The results from chloride permeability tests on virgin specimens may be used as a basis for comparison of tests performed on the in-situ pavement in the future after deicing salts have been used under service conditions.

Table 5.2 – RCPT results for specimens tested at 28 days of moist curing and 112 days of moist curing

Specimen	28 Day Charge (Coulombs)	112 Day Charge (Coulombs)
1	3,807	3,177
2	3,770	3,245
3	4,203	3,015
4	3,896	3,168
5	4,265	
6	4,082	
7	3,976	
8	4,179	
9	3,819	
Average	**4,000**	**3,150**

5.2.4. FREEZE – THAW RESISTANCE

The four prisms cast for freeze-thaw testing were subjected to a total of 315 cycles. Figure 5.9 shows the decrease in relative modulus with increased number of freeze-thaw cycles. No readings were taken between 250 and 315 cycles, because the researchers responsible for taking the readings were installing instrumentation in panels at the precasting yard in Memphis, TN. The average total degradation in modulus of elasticity was 3%. From these results it can be assumed the concrete mix is very durable when subjected to cycles of freezing and thawing. This is a result of a proper air void system, sound aggregates, and a low water to binder ratio.

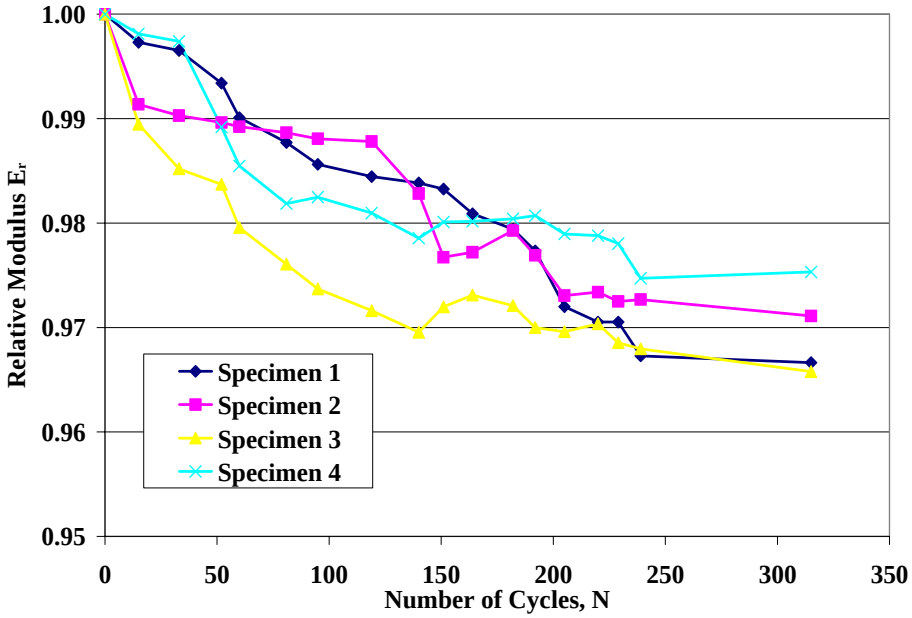

Figure 5.9 – Experimental results for freeze-thaw tests showing the degradation of modulus versus the number of cycles

5.2.5. FLEXURAL STRENGTH AND FRACTURE ENERGY

A total of two prisms were tested in flexure at an age of 56 days. Figure 5.10 shows the load versus deflection response for the two prisms. The net and gross deflections are both measured and shown in Figure 5.10. The gross deflection for the two beams is five times greater than the net deflection, which is mainly due to local concrete crushing at the supports of the testing apparatus. The amount of energy absorbed versus deflection is plotted in Figure 5.11.

Results calculated are based on the net deflection values obtained during the experiments and are summarized in Table 5.3. The average modulus of elasticity from the flexural tests was 5.33 x 10^6 psi (37 GPa). This modulus is 15% lower than the average modulus obtained from the compressive strength tests. The average modulus of rupture for the two prisms was 872 psi (6.0 MPa) and the average fracture toughness for

the concrete was 0.237 lb-in/in^2 (41.2 N-m/m^2). There was a significant variation in the results for the fracture toughness due to the limited number of prisms tested and the inherent scatter in this property.

Table 5.3 – Summary of results from flexural tests performed at 56 days

Specimen Number	Modulus of Elasticity, E_c psi (GPa)	Modulus of Rupture, R psi (MPa)	Fracture Toughness, G_f lb-in/in^2 (N-m/m^2)
1	5,550,000 (38.3)	798 (5.50)	0.211 (36.7)
2	5,110,000 (35.2)	946 (6.52	0.263 (45.8)
Average	5,330,000 (36.7)	872 (6.01)	0.237 (41.2)

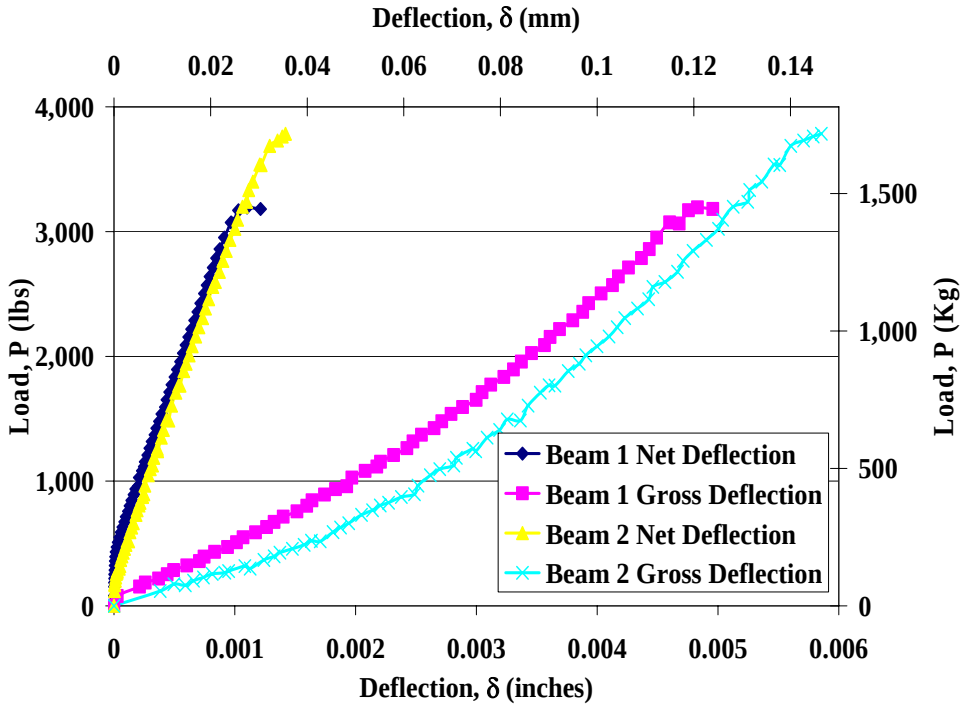

Figure 5.10 – Load versus deflection results for flexure tests of concrete prisms at an age of 56 days

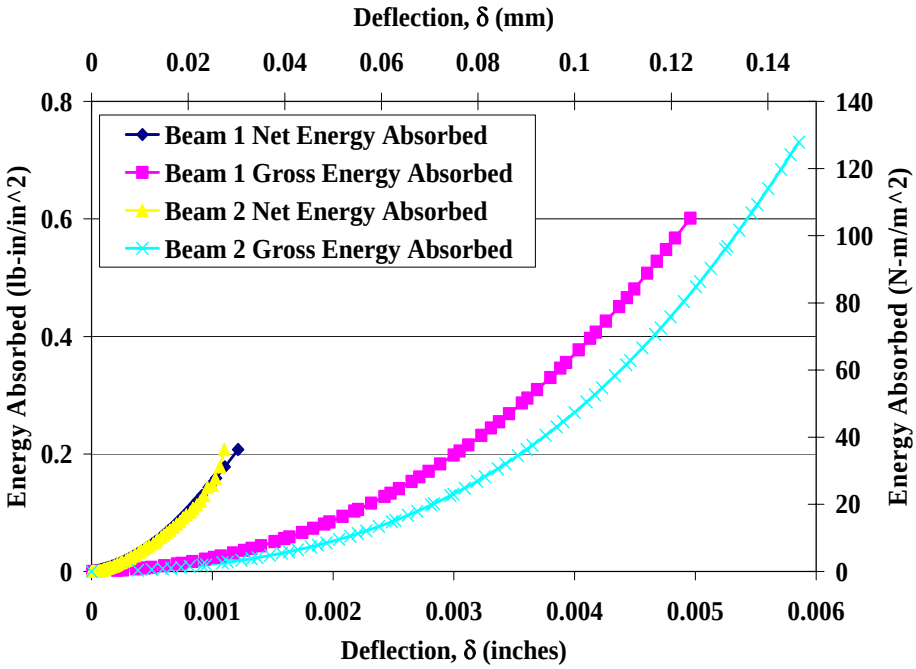

Figure 5.11 – Energy absorbed in concrete prisms during flexure tests

5.3. MATERIAL PROPERTIES OF STEEL CONSTITUENTS

The following sections detail the types of steel used in the precast panels. Knowledge of mechanical properties of the constituent materials is essential in determining the structural response of the prestressed concrete system.

5.3.1. PRESTRESSING STEEL STRANDS

All prestressing steel strands were seven-wire, uncoated, low-relaxation strands with ultimate strengths of 270 ksi (1860 MPa). Two sizes of prestressing steel were used in this PPCP project. Pre-tension steel utilized 0.5" diameter strands (A_{strand} = 0.153 in^2 (1 cm^2)) and stressed to 75% of ultimate strength. Post-tensioning steel strands were 0.6" diameter (A_{strand} = 0.217 in^2 (1.4 cm^2)) and stressed to 80% of ultimate strength. Pre-tensioning and post-tensioning steel strands were crossed above and below each other

alternately to prevent eccentricity of the compressive force being applied to the concrete placed around them. Figure 5.12 shows already stressed pre-tensioning strands along with the post-tensioning ducts.

Figure 5.12 – Pre-tensioning strand layout with post-tensioning ducts installed

5.3.2. CONVENTIONAL STEEL REINFORCING BARS

All conventional reinforcing bars used in the project were epoxy coated, grade 60 steel. Two epoxy coated #4 rebars were used around the perimeter of all base panels. These bars were secured in place with chairs or wall mounts that fastened to the edge of the forms.

Joint panels required sophisticated designs to transfer the massive prestressing forces from the steel strands into the pavement. Over ¼ of a mile of #4 rebar was used in each of the joint panels, the majority of which being located around the blockouts for the post-tensioning strands. Figure 5.13 shows the cross section details of the complex joint panels and indicates a few of the materials used. More detailed specifications can be found in Appendix A. Estimated quantities of reinforcing steel for each joint panel can

be seen in Table 5.4. Figure 5.14 shows the matrix of conventional rebar reinforcement required around each of the post-tensioning blockouts.

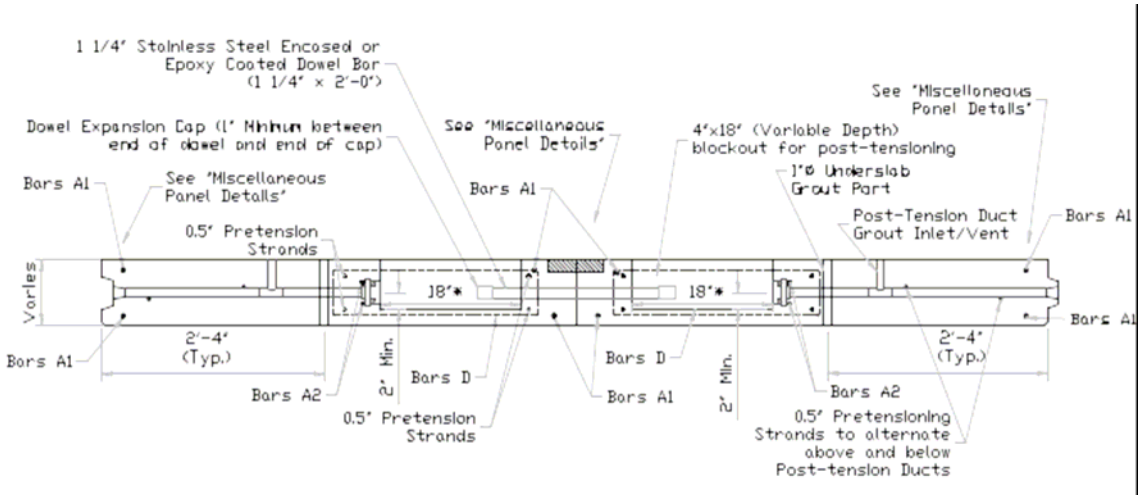

Figure 5.13 – Cross section of joint panels indicating steel details (Transtec 2005)

Table 5.4 – Estimated quantities of conventional rebar used in joint panels designs (Transtec 2005)

TABLE OF ESTIMATED QUANTITIES				
Bar	No.	Size	Length	Weight
A1	8	#4	37'-7"	201
A2	4	#4	35'-4"	94
C	4	#4	2'-11"	8
D1	120	#4	5'-3"	421
D2	38	#4	5'-1"	129
D3	20	#4	4'-11"	66
U1	4	#4	7'-0"	19
U2	4	#4	7'-3"	19
Reinforcing Steel			Lb	957
Class '*' Concrete			CY	10.1

Figure 5.14 – Conventional epoxy coated rebar used extensively to reinforce region where post-tensioning force will be applied in joint panels

Thirty-seven epoxy coated dowel bars were used to span between the joint on the joint panels (1.25” diameter x 2’0” long). They were located 1’ on center and coated with grease to prevent adhesion to the fresh concrete. Figure 5.15 shows the dowel bars with black expansion caps installed between the reinforcement required for stress transfer from the post-tensioning steel. Figure 5.16 shows the first set of grout ports for the section and the lifting pots used to handle the panels. The lifting pot has a green plastic space holder to prevent concrete from filling the threaded portion of the device.

Figure 5.15 – Epoxy coated dowel bars with expansion caps installed

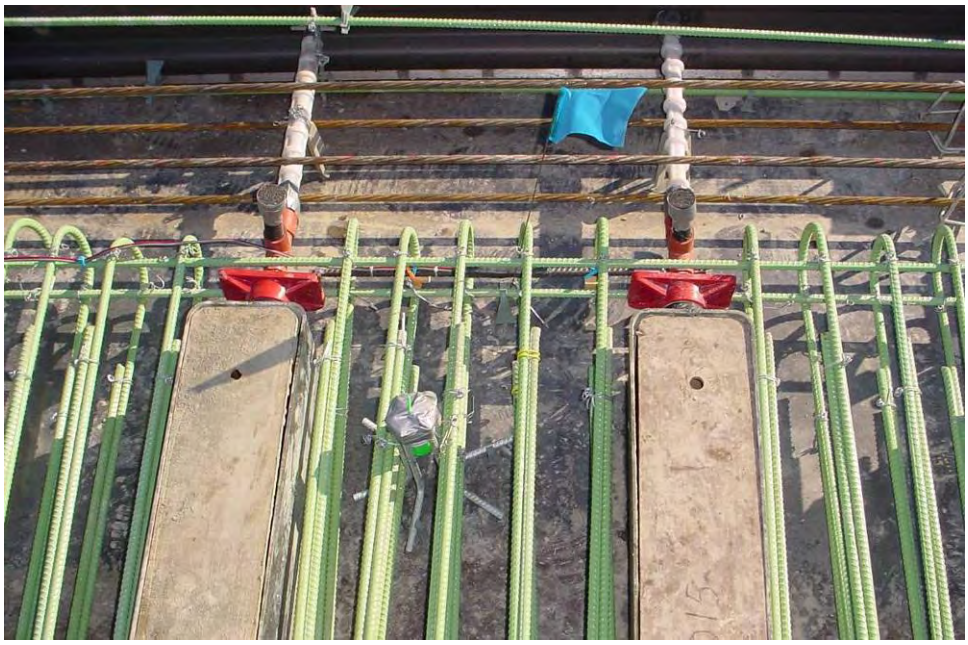

Figure 5.16 – Connection details of block outs and lift points

This page intentionally left blank.

6. EARLY AGE RESPONSE

6.1. CURING & HYDRATION

Analysis of hydration and early age response of reinforced concrete is a difficult task. Prediction of coupled thermal and mechanical behavior with phase transition from liquid to solid becomes complex and is affected by the following phenomena:

- Concrete changes thermal properties (namely expansive) as it transitions from plastic to solid (Kada H. 2002; Earney, Gopalaratnam et al. 2006).
- Hydration is an exothermic reaction which adds heat to system under consideration (Eatherton 1999).
- As concrete hydrates it shrinks (Earney, Gopalaratnam et al. 2006). This is counterintuitive to the fact that the system heats during hydration.
- While the concrete shrinks the steel will continue to expand with added heat (Shackelford and Alexander 2001).
- Steel expands and contracts at a relatively better understood linear thermal coefficient that happens to be roughly twice that of hardened concrete (~12 μstr/°C steel compared to ~6 μstr/°C limestone concrete) (Shackelford and Alexander 2001).
- Small amounts of friction from external steel formwork resist thermal movements as well as apply stresses to the outer surface during differential expansion.
- Thermal gradients develop through the depth of the cross-section causing corresponding internal strain gradients

- Differences exist between instantaneous and steady-state thermal response of the rebar and surrounding concrete. The concrete (with a very large surface area) heats and responds to thermal changes at a different rate than that of the embed rebar.

The analysis is further complicated by strain measuring devices such as vibrating wire strain gages that have their own unique thermal behavior affecting observed behavior. Vibrating wire strain gage output in plastic concrete is likely to be influenced by changing restraints as concrete hardens. It is for these reasons that instrumented rebar strains during "Curing and Hydration" are reported in their raw form as, "rebar strain" as opposed to concrete strain. Explanation for the calculation of concrete strains from rebar strain for hardened concrete is included in Section 6.1.3. The following sections discuss the theoretical predictions (based on idealized analysis of thermal changes), thermal data, and strain data in conjunction with hydration and external conditions such as steam curing and ambient temperature changes.

6.1.1. THEORETICAL PREDICTIONS

Theoretical estimates shown on the figures in this chapter are based strictly on thermal predictions developed from a tri-linear model of the Coefficient of Thermal Expansion (CTE) of curing concrete. The theoretical curves have been idealized to show predictions based on the thermal expansion and contraction of the concrete and rebar. They allow for an approximate comparison between the magnitudes of strains measured and those expected under ideal conditions. The following equation was used to calculate the expected thermal strain of hydrating concrete:

$$\Delta \varepsilon_{Thermal\ /\ Concrete} = CTE_{Concrete} \times (T_1 - T_0) \qquad \textbf{6.1}$$

'T' represents temperature at two distinct times (t_1 and t_0). The 'CTE' is the Coefficient of Thermal Expansion based on the tri-linear model from Kada, shown in Figure 6.1. Early age thermal gradients were small; therefore, an average temperature was used to simplify the analysis. The tri-linear CTE model shows that concrete behaves much like a fluid in its plastic state. After estimated initial set it begins transitioning to solid state (estimated final set) where it retains these thermal properties for the life of the composite (Kada H. 2002; Earney, Gopalaratnam et al. 2006). Kada's model was modified for the Missouri concrete based on known thermal data for local limestone aggregate (CTE of 6 μstr/°C).

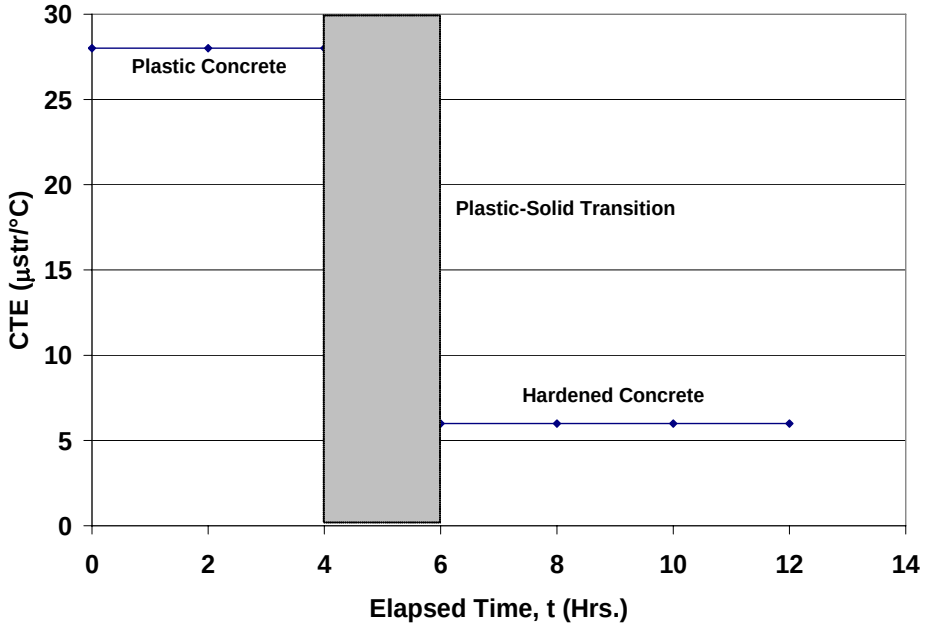

Figure 6.1 - Coefficient of thermal expansion assumed for curing concrete (Kada H. 2002)

6.1.2. MEASURED TEMPERATURES

Figure 6.2 summarizes the average curing temperatures for each panel. Panels B1 and B2 curing temperatures are lower (on average) than the rest. These temperature

histories are attributed to the fact that steam environment temperatures averaged 34°C (93°F) in Panels B1 and B2 and 54°C (129°F) in the rest of the panels. The temperature history shown for Panel A32 is shaped differently because it started at a lower ambient temperature and increased rapidly when the steam curing started. Average ambient temperatures for Panels B1, B2, B3, B4, and C1 were around 20°C (68°F). Panel A32 was cast in December and had an average ambient temperature of 8°C (46°F). Based on the relative steam curing environment temperatures, it can be inferred that Panel A32 was insulated much better than Panels B1 and B2. CPI used a double tarp during joint panel casting in mid December, 2005.

Maximum measured curing temperatures were 5-10°C (9-18°F) greater than the external steam curing environment temperatures (see Figure 6.6 and Figure 6.7). This higher temperature, beyond external heat sources (steam), can be attributed to exothermic hydration of the cement (Eatherton 1999). This trend was typical in nearly all instrumented panels.

Figure 6.3 shows the curing temperatures in joint Panel A32 as measured by thermocouples and vibrating wire thermistors. The temperatures shown are a snap-shot summary of near peak temperatures during curing of the second half of Panel A32.

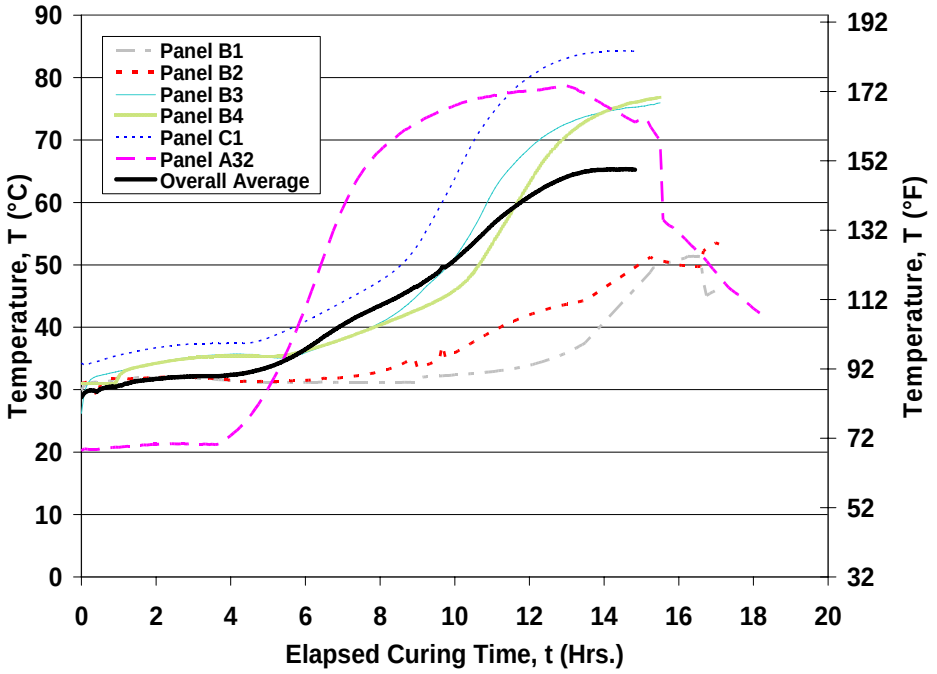

Figure 6.2 - Summary of average curing temperatures in each panel

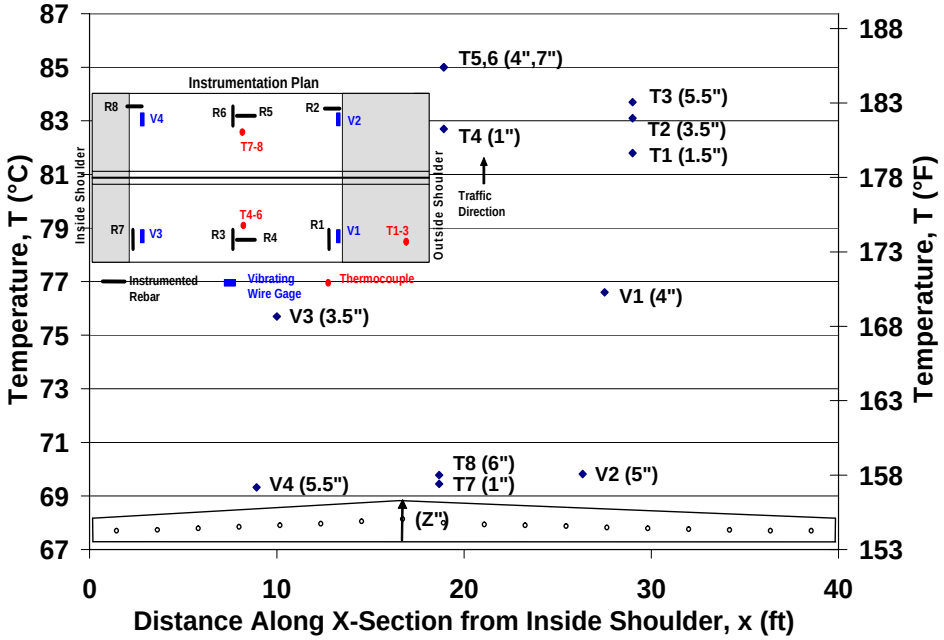

Figure 6.3 - Early-age temperatures in the cross-section of Panel A32

There was very little difference in Thermocouples T1-6. These are located within the un-cured plastic half of Panel A32. Thermocouples T5 and T6 have slightly higher temperature readings than adjacent measurements from Thermocouples T1-3. This is

because they are toward the center, within a larger thermal mass (deeper section of the location).

The vibrating wire gage thermistors are encapsulated in a hardened resin that insulates the sensor and makes it less sensitive to dynamic changes in temperature. Since the concrete is changing temperature rapidly, vibrating wire measurements appear to "lag" behind the thermocouples.

The average temperature of these six thermocouples is 83.4 °C (182°F) with a standard deviation of 1.5 °C (2.7°F). If it is assumed that the concrete has a CTE ranging between 6-8 μstr/°C, then these small differences in temperature create a strain gradient less than 15 μstr. This is very small compared to the overall strains during curing (less than 3%). These residual strain gradients, if large enough, can be responsible for premature cracking (Emborg and Bernander 1994), (Gopal et al 2001).

The temperature sensors in the cured first half of the panel report lower temperatures than the uncured second half. The external temperature is the same for both the cured and uncured halves. The difference in temperatures reinforces the previously stated effect that the heat from hydration of cement is increasing the curing temperature. The temperature difference reported by T1-6, V1, and V3 due to heat of hydration is roughly 13°C (23°F). Figure 6.6 shows the differences between the internal temperature of the cured and uncured sections.

Collectively, temperature sensors performed satisfactorily, displaying accurate and consistent trends. Note that ambient and steam curing environment temperature histories were recorded during each casting.

6.1.3. MEASURED CURING STRAINS

Instrumented rebars and vibrating wire strain gages were continuously monitored during curing hydration. Before hardening, the concrete is plastic and able to flow like a liquid. After hardening the concrete is solid with time-dependent strength and stiffness development. Strains are at best defined in a nebulous manner when concrete is in this early age transition (Eatherton 1999). Strains recorded during these early ages are hence termed "apparent strains" to highlight this fact. However, it is interesting to study relative strain development compared to measured curing temperature at these early ages when hydration and liquid to solid transition takes place. Even if true strain magnitudes during these early ages cannot be established with certainty due to the phase transition, *relative* magnitudes, and trends offer valuable information on potential distributions of stresses. The apparent strain in the instrumented rebar and vibrating wire strain gages show what types of strains are induced in these gages by movement in the concrete and therefore *relative* magnitudes and peaks (in conjunction with curing temperatures) provide useful information. In all strain graphs, compressive strain is represented as a negative strain value and tension as a positive strain value (this convention is valid for all plots in this report).

It is important to note that the two theoretical curves represent expected concrete and rebar strain. Rebar readings are measured rebar strain. To convert measured rebar strain into estimated thermal concrete strain the following equation is used:

$$\Delta\varepsilon_{Concrete} = \left(\frac{CTE_{concrete}}{CTE_{concrete} - CTE_{rebar}} \right) \times (R_1 - R_0) \qquad \textbf{6.2}$$

The 'R' values are reported rebar strain. The CTE for steel rebar is larger than that of concrete (Shackelford and Alexander 2001). The first part of this equation creates

a negative scalar value that is multiplied with measured rebar strain (R_1-R_0). Equation 6.2 is obtained by: consider as the idealization.

1. An unrestrained (no concrete) instrumented rebar of length L is heated and allowed to expand to a length of $L+\Delta L_{us}$.
2. The strain reading will remain zero as the gages on the rebar are self-temperature compensational for steel and are also in a full-bridge configuration.
3. Embedding the rebar in concrete (Figure 6.4) provides restraint on this free expansion.
4. Therefore, although the total displacement (ΔL_r) of the instrumented rebar is positive (extension), it exhibits compressive strain for restrained expansion of: $(\Delta L_{us}-\Delta L_r)/L$.

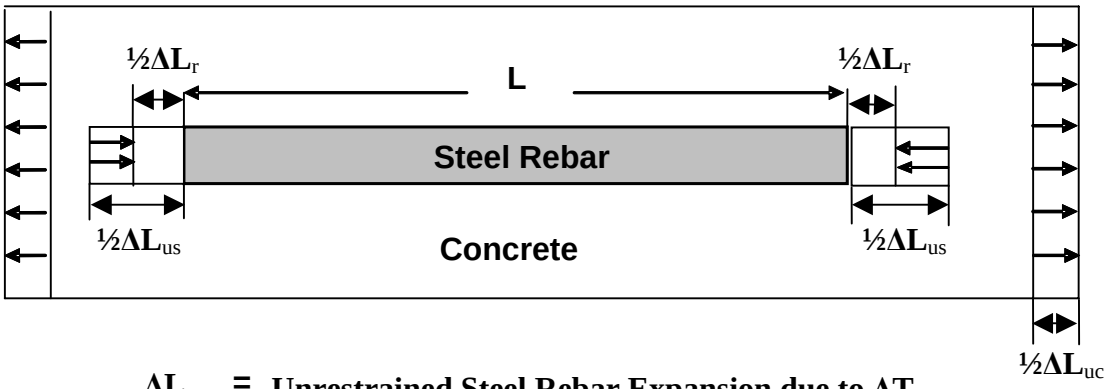

ΔL_{us} = Unrestrained Steel Rebar Expansion due to ΔT

ΔL_r = Restrained Steel Rebar Expansion due to ΔT

ΔL_{uc} = Unrestrained Concrete Expansion due to ΔT

Figure 6.4 - Restraint of instrumented rebar by surrounding concrete

For all six panels instrumented (with both thermal and strain measuring devices), the trends in apparent strain and temperature are related. Panel A32 is unique in that it was monitored over several days. The first half was cast on Friday, December 9, 2005.

The panel was monitored all weekend and the second half was cast the following Monday, December 12, 2005. Figure 6.5 shows the entire curing strain history of Panel A32 from casting of the first half to stress transfer. The instrumented rebars go into compression during curing of the first half. This is an expected result of shrinkage and restrained thermal expansion of the rebar in the concrete. At roughly 10 hrs, the temperature begins to drop. This is marked by a gain in tensile strain due to thermal contraction (the rebar contracts more than the concrete will allow—showing tensile strain).

During casting of the first half, maximum compressive rebar strains occur at the highest curing temperatures (which happen to be higher than steam curing environment temperatures). Theoretical strains are lower magnitude because unlike the measured strains, there do not account for added compressive strain due to shrinkage (difficult to quantify at early age). The difference between theoretical thermal rebar strain and measured strain is 200-300 μstr (Figure 6.5). As stated earlier, the theoretical curve is based solely on the coefficient of thermal expansion. It proves to be useful as it shows the same shape and trend as the measured apparent strains, implying that a significant component of the recorded response is due to thermal loading. Up until curing of the second half, each action causing thermal (steam off, tarp removed) can be seen with subsequent changes in temperature and related strains.

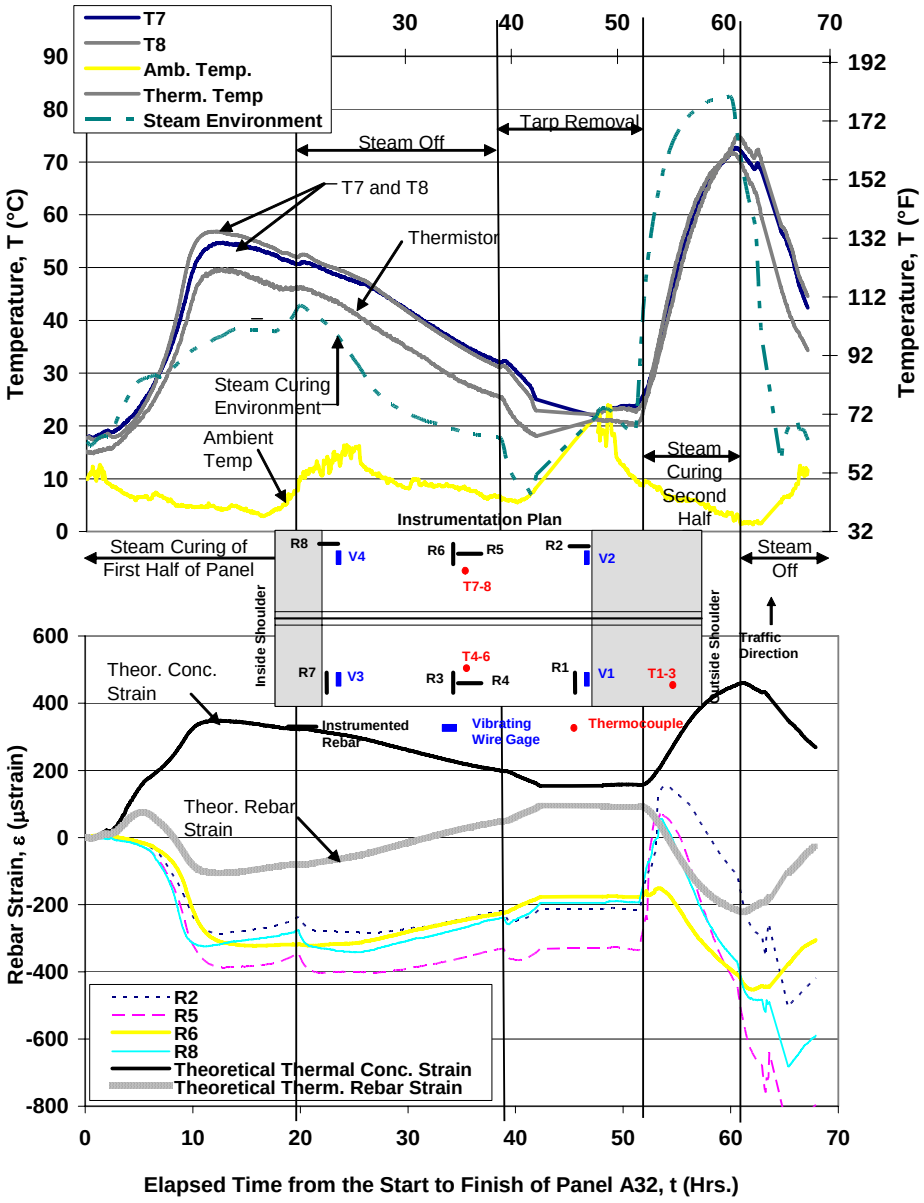

Figure 6.5 - Early-age thermal strain history of 1st half of Panel A32 through completion of 2nd half (a) temperature history, (b) strain history

The shape of the theoretical rebar strain curve matches measured rebar trends—especially Rebar 6 (Figure 6.5 and Figure 6.6). Rebar 6 is the only transverse rebar in the first half of Panel A32. It shows a different trend during curing of the second half (hour 53—Figure 6.5 and hour 5—Figure 6.6) than longitudinal rebar (Rebar 2, 5, and 8 in Figure 6.5 and Figure 6.6). The sharp jump in tensile strain seen in the longitudinal rebar

is not visible in strain readings from Rebar 6. This may be due to a difference in external restraint in the long direction from the formwork. It is speculated that the level of formwork restraint is different in the longitudinal and transverse directions.

To explain this sharp jump further, Figure 6.6 shows all of the rebars in Panel A32 and their comparative response during curing of the second half. This graph includes part of response shown in the last half of Figure 6.5 for Rebar 2, 5, 6, and 8 in addition to response from rebar in the curing second half. The rebars in the hardened first half show signs of expansion as soon as steam curing starts for the second half. The differences between rebar subjected to curing strains and those under solid-state thermal response are highlighted. When steam curing begins (4 hrs) the instrumented rebars in the plastic second half of Panel A32 indicate compression which reflects the bonded thermal behavior described previously. The rebar in the solid first half expand and then fall into compression as noted earlier. Based on the earlier discussion with respect to thermal strains, the rebar should go into compression because the steel expands more than the concrete will allow. The exception shown in Figure 6.5 and Figure 6.6 (with hardened concrete) can be attributed to the difference in thermal mass as well as delays in attainment of steady state temperature throughout the panel and instantaneous thermal gradients between the embedded rebar and other concrete.

When the steam is turned on, the concrete is instantaneously ‘shocked’ with a thermal load. The concrete mass around the rebar quickly begins to heat and expand before the temperature of the steel bar can ‘catch up’ and reach a similar steady-state condition. Therefore, due to this delayed response, the concrete pulls the rebar into

tension. In time, the rebar expands and exhibits compression as expected. The fact that theoretical values are close for both halves also supports this theory.

This effect can be seen in the hardened concrete because plastic concrete does not have the bond strength to fully restrain the rebar. It is also likely that the formwork providing more restraint in the long direction, mitigating this effect on Rebar 6 somewhat.

shims (some of them made of steel) make concrete strains non-uniform. Panels B1, B2, and B3 show higher strains near the right side. Generally, strains from Rebar 1, 2, and 4 are higher opposite the active jacking end (east side) and decrease as the panels get closer to the jack (Figure 7.5, Figure 7.6, and Figure 7.7 respectively). Strains in Panel B3 are generally the highest then progressively decrease at Panels B2 and B1 respectively.

Although the active stressing end is at the Panel A31 side of Section 3, higher strains were created at the opposite end first (eastern). This hypothesis is best represented by comparing relative strain magnitudes from Rebar 2, Rebar 4, and Rebar 5 for all instrumented panels. This occurred because the section was anchored at the active jacking end (western or Joint A31). As the panels were stressed the gaps were filled from east to west (from Panel A32 to Panel A31). Sections 1 and 2 had already been stressed. None of the joint panels opened during stressing. Section 4, on the other side of Panel A32, was not attached. Therefore the point of least resistance was at Panel A32. Starting at Joint Panel A32 the slabs moved from right to left toward Panel A31. Because the strands slid through each panel, the main active force was from the bearing in Joint Panel A32, ultimately creating higher stresses at Panel B3. Frictional resistance then increased toward Panel A31 and the measured rebar strains became progressively lower from right to left as shown in Figure 7.10.

The effect of service temperatures on prestressing force is also of interest from a performance point of view. Figure 8.18 includes a plot of temperature (ambient and pavement temperature at crown at mid-height where the post-tensioning strandmeter monitored is located) and associated strandmeter strain history recorded in Panel C1. If the post-tensioning strand was unbonded, one would expect strand strain to decrease with a decrease in pavement temperature due to elastic shortening of the pavement section. However, since the post-tensioned strands are grouted, they behave as if they were bonded, with a decrease in temperature producing tensile strains in the strand instead (Figure 8.18b, due to prestressing steel which has a higher CTE being restrained by concrete with a lower CTE – thus producing compression in concrete and tension in steel for the incremental temperature event). Notice that Figure 8.18b shows actual strandmeter strain magnitudes (i.e. uses the actual zero strain reference from the start of the post-tensioning operations, rather than a dummy "zero strain reference" to highlight effect of the temperature event alone). The loss in prestress from when the post-tensioning operations were completed includes losses due to initial elastic shortening, friction, creep, shrinkage and relaxation (see also Figure 7.12 for magnitude of strand strain in Panel C1 immediately following post-tensioning operations).